A SIMPLE AND EFFICIENT MODEL FOR SEISMIC RESPONSE AND LOW-CYCLE FATIGUE ASSESSMENT OF UPLIFTING LIQUID STORAGE TANKS

A SIMPLE AND EFFICIENT MODEL FOR SEISMIC RESPONSE AND LOW-CYCLE FATIGUE ASSESSMENT OF UPLIFTING LIQUID STORAGE TANKS[1]

Maria Vathi [a] and Spyros A. Karamanos [a, b, 2]

[a] *Department of Mechanical Engineering, University of Thessaly, Volos, Greece*

[b] *Institute of Infrastructure and Environment, School of Engineering, The University of Edinburgh, Scotland, UK*

ABSTRACT

Ground-supported unanchored liquid-storage cylindrical tanks, when subjected to strong seismic loading may exhibit uplifting of their bottom plate, which may have significant effects on their dynamic behavior and structural integrity. In particular, due to uplifting, a substantial amount of plastic deformation develops at the vicinity of the welded connection between the tank shell and the bottom plate that may cause failure of the welded connection due to fracture or fatigue, associated with loss of tank containment. The present study focuses on the base uplifting mechanism and tank performance with respect to the shell/plate welded connection through a numerical simple and efficient methodology that employs primarily a simplified modeling of the tank as a spring-mass system for dynamic analysis, enhanced by a nonlinear spring at its base to account for the effects of uplifting, supported by a detailed finite element model of the tank for incremental static analysis. The latter model is capable of describing with accuracy the state of stress and deformation at different levels of lateral loading, in order to obtain the overturning moment-rocking angle relationship to be used in the simplified model. The methodology is applied in two cylindrical liquid storage tanks of different aspect ratios focusing on

[1] *Submitted for SPECIAL ISSUE on Risk Analysis in the Process Industries: State-of-the-art and the Future*

[2] *Corresponding author. Email: spyros.karamanos@ed.ac.uk*

local performance of the welded connection, towards assessing the strength of the welded connection. The numerical results provide better understanding of tank uplifting mechanics and strength against failure of the welded connection at the tank bottom. Furthermore, the proposed methodology can be used for efficient assessment of uplifting effects on tank structural safety, towards minimizing seismic risk in industrial facilities.

1. INTRODUCTION

Liquid containing tanks made of steel material are used in water storage and distribution systems, as well as in industrial plants for storage and/or process of a variety of liquids and liquid-like materials, including oil, liquefied natural gas, chemical fluids and wastes of various forms. In numerous practical applications, relatively broad aboveground liquid storage tanks are constructed unanchored, in the sense that their bottom plate is in simple contact with the ground, without any anchor bolts. Under strong lateral dynamic loading (e.g. seismic), these tanks may exhibit uplifting of their bottom plate, when the magnitude of the overturning moment exceeds a threshold value. Although uplifting does not necessarily result in tank failure, its consequences may lead to serious damage of any attached piping connections of the uplifted bottom plate, and possible failure of the connection between the tank shell and the bottom plate [1][2]. Furthermore, it may result in an increase of the axial stress acting on the tank wall, which may lead to occurrence of "elephant's foot" buckling at lower uplifting sizes [3]. This behavior is shown schematically in Figure 1; for the direction of lateral loading shown in the sketch, Location 1 is the critical location of concern in the present paper, associated with tank uplifting.

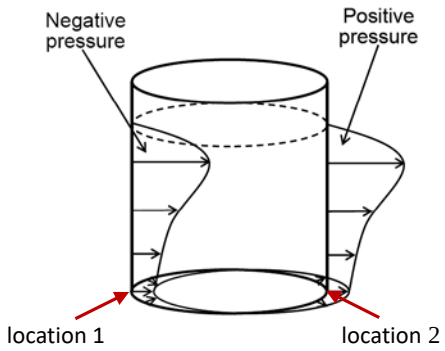

Figure 1: Locations affected by uplifting during seismic action in an unanchored tank.

The uplifting response of tank base plate is nonlinear due to continuous variation of the base contact area, plastic yielding of the plate material, and the effects of membrane forces associated with large displacements in the plate. A first attempt to understand the uplifting resistance mechanism of a plate has been reported, solving the simple problem of a prismatic beam uplifted at one end [4][5], ignoring the effect of membrane forces in the base plate; it was found that the maximum load capacity of the beam is reached at the stage where two plastic hinges develop: one at the uplifted end (i.e. at the shell-plate connection), and the second at the "sagging moment" region of the beam model [4][6], shown in Figure 2. An approximate solution that accounts for the effects of the membrane forces was proposed by Cambra [7] using simplifying assumptions regarding the magnitude of the axial and shearing forces in the beam based on experimental data from axially symmetric lift, static tilt and dynamic shaking table tests. Auli *et al.* [8] employed a second-order beam theory that accounts more accurately for membrane forces, however their methodology did not account for the effects of flexible end conditions of the beam nor for plastic yielding within the beam. Ishida and Kobayashi [9] used finite element models to solve the uplifting problem as an uplifting beam under rocking conditions. Malhotra and Veletsos [10] studied extensively uplifting behavior, idealizing the base plate as a uniformly-loaded semi-infinite prismatic beam on a rigid foundation, considering the effect of elastic end constraints, the influence of

the axial force on bending and the effect of plastic yielding in the beam. In a recent publication, Ahari *et al.* [11] used a tapered beam model resting on a rigid foundation to simulate base uplift of unanchored tanks and investigated the parameters which are affecting it.

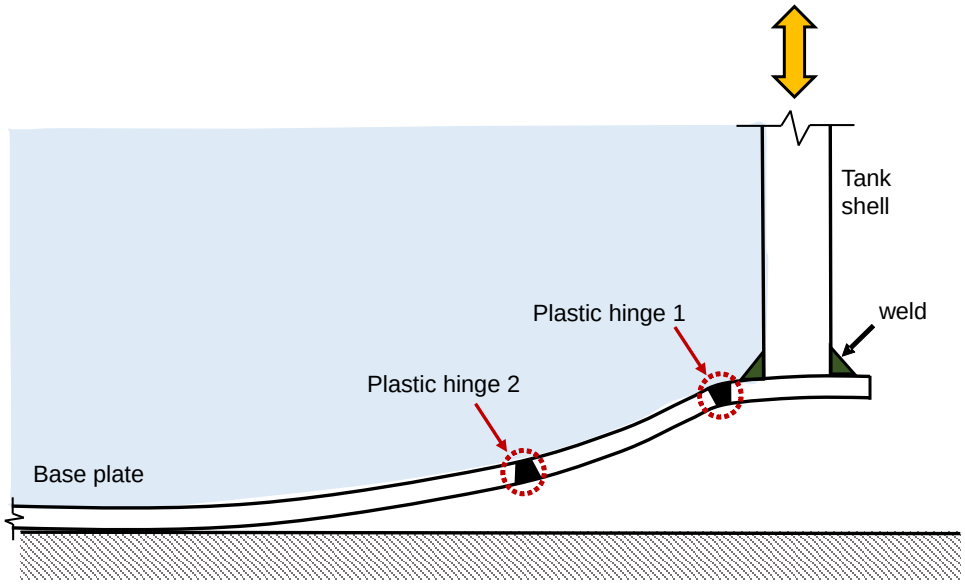

Figure 2: Locations where plastic hinges develop on the base plate; (1) at the shell-plate connection; (2) at the "sagging moment" region.

The aforementioned beam models did not take into account the two-dimensional nature of the problem under consideration, neglecting the effect of hoop stresses, which develop in the base plate close to the junction of the bottom plate with the tank wall. A fundamental step towards understanding uplifting in liquid storage tanks has been the consideration of a partially-uplifted base plate model. Such studies have been reported in [12][13] using a combination of the finite-difference solution method and energy method, whereas the Ritz energy method has been employed in [14][15]. Malhotra and Veletsos [16] have improved the "plate model" approach computing the vertical uplift and rocking resistances of a circular plate to uniformly uplifting forces distributed along its boundary, presenting

solutions methodologies for axisymmetric vertical uplifting, as well as for asymmetric rocking uplifting, using a series of semi-infinite prismatic beams.

Apart from the above analytical models, notable experimental works for the behavior of unanchored fluid-filled tanks have been performed in the 80's at UC Berkeley [17][18][19][20]; they refer to shaking table and static tilt tests. Furthermore, Shih [21] reported scale model tests in an effort to obtain a better understanding of the response and the failure mechanism of the tanks. In subsequent publications, Natsiavas [22][23] and Natsiavas & Babcock [24] presented analytical models for determining the dynamic response and the hydrodynamic loads developed on unanchored liquid-filled tanks under horizontal base excitation. More recently, Malhotra and Veletsos [25], based on their previous works [10][16], investigated the effects of uplifting of the bottom plate of the tank on the entire tank-liquid system, for a rigid foundation using a simplified model.

The present study examines the uplifting mechanism of tank bottom subjected to seismic loading and its effects on tank structural integrity, using numerical simulation tools. Two typical liquid storage tanks are modeled using finite elements, both anchored and unanchored, and their behavior is discussed considering also the relevant seismic provisions in EN 1998-4 [26]. The main purpose of the present study is the proposal of a simple and efficient methodology for the analysis and design of the shell-bottom plate connection, where fracture may occur due to the development of excessive tensile strain or low-cycle fatigue, and lead to loss of containment [27]. More specifically, a simplified analytical model for dynamic analysis is developed, accounting for uplifting. This simplified numerical methodology enhances the model proposed in [25], and is capable of calculating the maximum local strain at the welded connection and assessing its ultimate strength and fatigue life. The proposed model uses the Stowell-Hardrath-Ohman formula for local yielding and is supported by a rigorous finite element model of the tank for the purpose of determining two basic uplifting parameters; the uplifting length L and

uplifting size w. The proposed methodology can be used as an efficient tool for conducting a performance-based design procedure, as described in [30][31], using the limit state capacities offered in [28], towards assessing tank strength and minimizing seismic risk in industrial facilities.

2. NUMERICAL ANALYSIS

The numerical model of unanchored tank analysis focuses on the effects of base plate uplifting, and consists primarily on a simplified, yet efficient, model for dynamic analysis calibrated with the use of a nonlinear finite element model for static analysis. The latter model is used to determine the relationship between the overturning moment and the uplifting angle, as well as the relationship between the uplifting size and length at the tank bottom. Both models are described in the following.

2.1 Nonlinear Dynamic Analysis

2.1.1 Model Description

The simplified model accounts for the hydrodynamic response of the tank-liquid system. The cylindrical liquid storage tank has radius R and filling height H and is excited by a horizontal base-ground seismic acceleration motion $\ddot{X}_g$. It can be shown that the motion of the liquid-container system can be expressed as the sum of the so-called "convective" and "impulsive" motions, respectively [42] [43]. The convective term is associated with sloshing of the liquid free surface, whereas the impulsive term represents the liquid motion that "follows" the moving container, and accounts for container deformation. Due to the fact that sloshing natural frequencies are substantially lower than the natural frequencies of the impulsive motion, the two motions can be considered as uncoupled [25][43].

Herein, for the sake of completeness, anchored tank modeling is briefly described first, followed by a detailed description of unanchored tank modeling which focuses on the calculation of local strain at the shell-bottom plate connection and its fatigue assessment.

2.1.2 Anchored Tanks

The tank-liquid system is modeled as a spring-mass system, as seen in Figure 3. The impulsive and convective motion of the liquid are modeled by assuming two linear oscillators with masses m_I and m_C at heights h_I and h_C respectively. The values of frequencies $\omega_{I,C}$, masses $m_{I,C}$ and heights $h_{I,C}$ depend on the tank aspect ratio [42], whereas for oil or water tanks, values of 0.5% and 5% can be considered for the damping ratio of the impulsive and sloshing motion ξ_I and ξ_C, respectively.

Consideration of additional sloshing modes is possible introducing additional linear oscillators, but their effects on the total seismic response may be not significant and they are omitted for the purposes of the present analysis [44]. More details on the above model for deformable steel tanks under lateral seismic loading can be found in the papers by Veletsos and Yang [43] and Ibrahim [42].

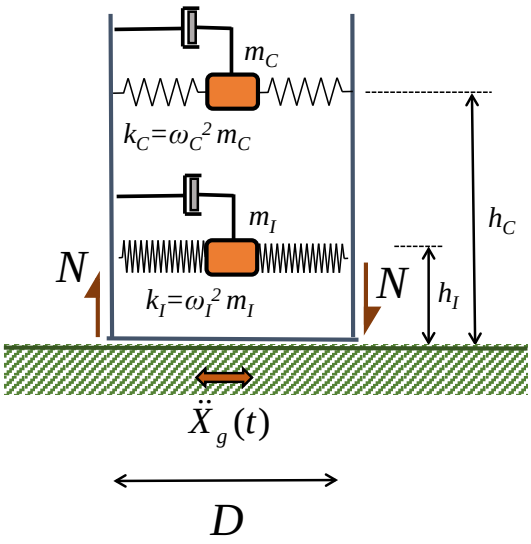

Figure 3: Simplified model for anchored liquid storage tanks.

The equations of motion have the form:

$$\ddot{a}_j(t)+2\xi_j\omega_j\dot{a}_j(t)+\omega_j^2 a_j(t)=-\ddot{X}_g(t), \qquad \text{where } j=I \text{ or } C \tag{1}$$

In the above equation, a_I and a_C are the impulsive and convective generalized coordinates, $\ddot{a}_I$ and $\ddot{a}_C$ are the corresponding accelerations and ω_I and ω_C are the impulsive and convective frequencies.

The total impulsive and convective accelerations of the system are calculated considering the following change of variables:

$$\ddot{u}_j(t) = \ddot{a}_j(t) + \ddot{X}_g(t), \qquad \text{where } j = I \text{ or } C \tag{2}$$

so that the overturning moment is calculated as follows:

$$M(t) = m_I \ddot{u}_I(t) h_I + m_C \ddot{u}_C(t) h_C \tag{3}$$

The maximum compressive or tensile force per unit circumferential length due to impulsive and convective motion is calculated from elementary structural mechanics:

$$N = \sigma t_s = \frac{M}{I} R t_s = \frac{1.273M}{D^2} \tag{4}$$

where t_s is the thickness of the bottom shell course. It is noted that the contribution of tank wall and roof inertia on the overturning moment, as well as gravity effects (liquid and tank) should also be considered.

2.1.3 Unanchored Tanks

The basic principles of the above model for anchored liquid storage tanks are also applicable in the unanchored case. However, base uplifting is the main new feature that should be accounted for. More specifically, the impulsive motion includes tank rotation ("rocking") due to uplifting, and is modeled by using an appropriate rotational spring at the tank base, shown in Figure 4. A first methodology to model this "spring" has been reported by Malhotra and Veletsos [25], and has been enhanced recently by Vathi and Karamanos [45][46][47]. A more updated version of the latter model is described in detail in the present paper. The key issue for accurate modeling is the relationship between the overturning moment M and the "uplifting" or "rocking" angle ψ, obtained through a nonlinear static analysis, as of the tank using a finite element simulation described in section 2.2.

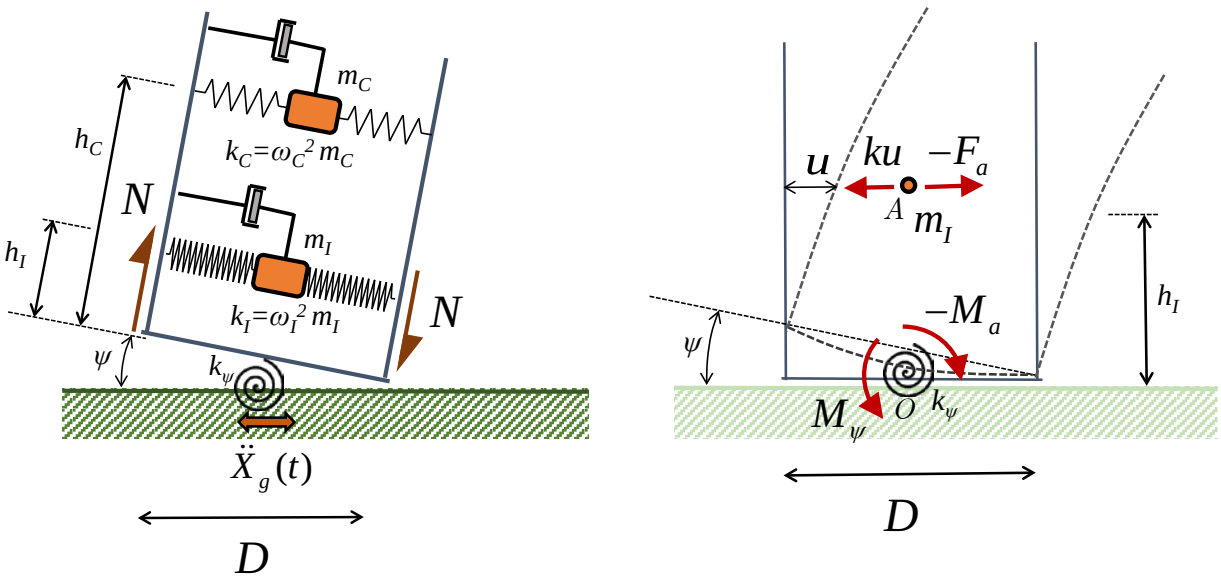

Figure 4: Simplified model for unanchored liquid storage tank; point O is the tank base center and point A is the center of the impulsive mass ("impulsive" center).

Because of the bottom rotational spring, the equations of motion (1) used in the anchored case have to be enhanced. The model has two degrees of freedom, the horizontal and the rotational motion of the tank. As stated earlier, it is assumed that the convective component of response can be uncoupled from the impulsive motion [25][43]. The former is rather small with negligible effects on the overturning moment and can be neglected, whereas the latter is modeled through a mass-spring model. Equilibrium of inertia and "elastic" forces in the horizontal direction requires:

$$F_a + ku = 0 \tag{5}$$

where constant k represents the stiffness of the oscillator, u is the top horizontal displacement of the tank and F_a is the force due to uplift of the tank so that the previous equation can be written:

$$m_I\left(\ddot{u} + \ddot{X}_g + \ddot{\psi} h_I\right) + ku = 0 \tag{6}$$

where $\ddot{\psi}$ is the rotational acceleration of the tank. Setting $k = \omega_I^2 m_I$ one obtains:

$$m_I\ddot{u} + m_I h_I\ddot{\psi} + m_I\omega_I^2 u = -m_I\ddot{X}_g \tag{7}$$

Furthermore, equilibrium of moments with respect to point O results in:

$$M_a + M_\psi + m_I h_I \left(\ddot{u} + \ddot{X}_g \right) = 0 \tag{8}$$

where M_a is the moment due to uplift of the tank, M_ψ is the moment due to the rotational spring at the tank base and $\ddot{u}$ is the horizontal acceleration of the tank. Therefore,

$$m_I h_I \ddot{u} + I_O \ddot{\psi} + M_\psi \left(\psi \right) = -m_I h_I \ddot{X}_g \tag{9}$$

where I_O is the rotational moment of inertia of the impulsive part of the liquid, computed with respect to the tank base plate according to Steiner's theorem as follows:

$$I_O = m_I \left(\frac{R^2}{4} + \frac{H^2}{3} \right) \tag{10}$$

and $M_a = I_O \ddot{\psi}$. Setting $\delta = h_I \psi$, equations (7) and (9) become:

$$m_I \ddot{u} + m_I \ddot{\delta} + m_I \omega_I^2 u = -m_I \ddot{X}_g \tag{11}$$

$$m_I \ddot{u} + \left(\frac{I_O}{h_I^2} \right) \ddot{\delta} + \frac{1}{h_I} M_\psi \left(\psi \right) = -m_I \ddot{X}_g \tag{12}$$

The equations are nonlinear because of the nonlinear spring resistance function $M_\psi \left(\psi \right)$ and can be written in incremental form as follows:

$$m_I \Delta\ddot{u} + m_I \Delta\ddot{\delta} + + c_1 \Delta\dot{u} + m_I \omega_I^2 \Delta u = -m_I \Delta\ddot{X}_g \tag{13}$$

$$m_I \Delta\ddot{u} + \left(\frac{I_O}{h_I^2} \right) \Delta\ddot{\delta} + c_2 \Delta\dot{\delta} + \frac{1}{h_I^2} K_\psi \Delta\delta = -m_I \Delta\ddot{X}_g \tag{14}$$

In the above equations appropriate damping terms have been added. In addition, $\Delta M_\psi \left(\psi \right) = K_\psi \Delta\psi$ and K_ψ is the tangent stiffness of the $M\left(\psi \right)$ function.

In equations (13) and (14), $c_1 = 2\xi_I m_I \omega_I$ is the damping coefficient for impulsive motion, associated with a damping ratio ξ_I, whereas $c_2 = 2\xi_O \sqrt{K_\psi I_O / h_I^4}$ is the damping coefficient for the rotational movement of the tank, where a damping ratio ξ_O of the uplifting motion is considered.

The system of equations (13) and (14) is solved using Newmark's method [48] considering the $M(\psi)$ function obtained from the nonlinear static analysis of the tank described in the next sub-section 2.2. The solution provides the values of lateral and rotational accelerations at each time increment, as well as velocities and displacements.

2.2 Nonlinear Static Analysis

Finite element program ABAQUS Standard is used for the simulation of the structural behavior of the tank under static loading, assuming both anchored and unanchored conditions (Figure 5). In the case of unanchored tanks, the tank shell and the bottom plate are modeled with shell finite elements, with special attention on the annular plate of the tank. More specifically, the tank and the bottom plate are modeled with four-node reduced-integration shell elements (S4R). In such a case, uplifting of the unanchored tank is simulated with the use of appropriate contact conditions between the bottom plate of the tank and the ground. The type of contact employed is referred to as "hard contact", which minimizes penetration of the slave surface into the master surface at the constraint locations and does not allow the development of tensile stress across the interface, whereas the two surfaces can be separated after contact at the beginning of the analysis to allow later uplifting of the bottom plate (Figure 5 and Figure 6). The friction coefficient between the tank base plate and the ground is assumed to be equal to 0.3. The ground is simulated using solid eight-node reduced-integration elements (C3D8R). The material of the ground is considered to be a material with density 7,500 kg/m^3, Young's modulus equal to 1.1×10^5 MPa and Poisson's ratio equal to 0.3. Finally, the tank roof is modeled with the use of two-node (linear) beam finite elements (B31). In the anchored tank case, the tank shell is simulated completely fixed (clamped) at its bottom.

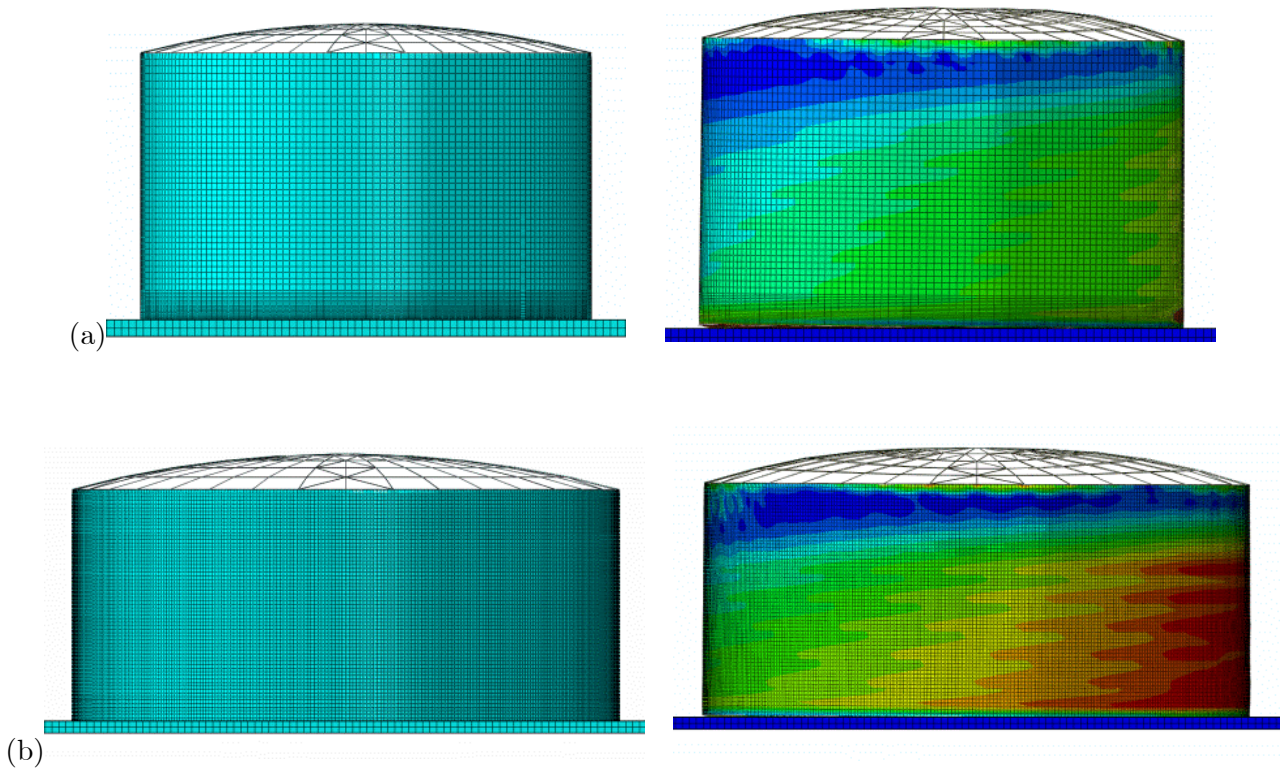

Figure 5: Finite element models of the two tanks under consideration, undeformed (left) and at the end of the analysis (right) with uplifting; (a) Tank I, (b) Tank II.

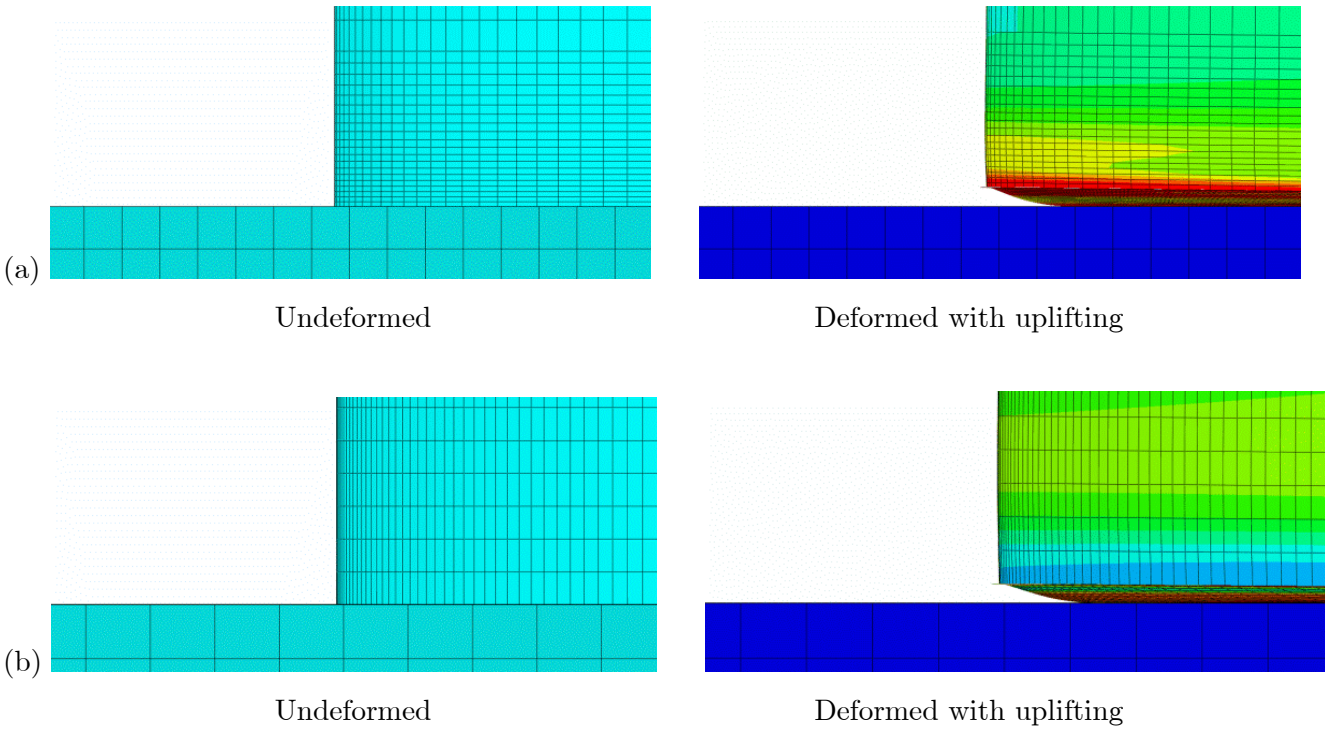

Figure 6: Uplifting of the bottom plate for (a) Tank I and (b) Tank II.

In the finite element model, the material of the tank is assumed to follow a von Mises (J_2) plasticity model, with isotropic hardening. The yield stress of tank and base-plate material is equal to 235 MPa, with Young's modulus of $E=$ 210,000 MPa, and hardening modulus equal to 210 MPa, which corresponds to 1/1000 of Young's modulus. An elastic material has been used to describe the ground with Young's modulus equal to half the Young's modulus of steel, implying practically non-deformable ground conditions.

The incremental non-linear static analysis is conducted in three steps. In the first step, gravity of the tank is applied, whereas in the second step, hydrostatic pressure of the liquid is activated. Finally, in the third step, horizontal hydrodynamic loading is applied, through an incremental elastic-plastic analysis with large displacements. The distribution of hydrodynamic pressure applied on the tank wall is assumed to follow the pressure distribution solution of the hydrodynamic problem [42], for both the impulsive and convective component of liquid motion [26][42]. More specifically, considering a cylindrical coordinate system, r, φ, z, with origin at the center of the tank bottom and vertical z axis, the distribution of hydrodynamic pressure for the impulsive motion is assumed in the following form:

$$P_I(\xi,\zeta,\theta,t) = C_I(\xi,\zeta)\rho H S_I \cos\varphi \tag{15}$$

where C_I is a spatial function of the non-dimensional coordinates $\xi = r/R$ and $\zeta = z/H$ of the tank which depends on the tank aspect ratio, ρ is the liquid density, H is the liquid height, R is the tank radius, and S_I is the impulsive acceleration. For the convective motion, only the first mode is considered.

$$P_C = 1.146R\rho\frac{\cosh\left(1.841\gamma\zeta\right)}{\cosh\left(1.841\gamma\right)}J_1\left(1.841\xi\right)S_C\cos\varphi \tag{16}$$

where J_1 is the Bessel function of first order and S_C is the convective acceleration. In the above expressions, r is taken equal to R ($\xi=1$) for determining the pressure on the lateral surface, whereas z is taken equal to zero ($\zeta=0$) for the pressure on the bottom plate.

The hydrodynamic pressure distribution is applied on the inner surface of the tank shell and at the bottom plate, using a special-purpose load-user subroutine in ABAQUS.

2.3 Calculation of local strain at the base plate connection

Upon calculation of the uplifting angle $\psi(t)$ from the solution of equations (13) and (14), and the corresponding overturning moment $M(t)$ using the $M-\psi$ relationship obtained from the static analysis, the uplifting displacement at the tank edge $w(t)$ can be computed equal to $D\psi(t)$, and the membrane meridional compression N is calculated from Eq.(4). Using this information, the maximum strain at the shell-plate connection can be estimated using an assumed-shape cosine function for the deflection of the base plate. More specifically, it is assumed that the plate deflects with transverse displacement w_1 along its radial direction in the following shape:

$$w_1(x)=\frac{w}{2}\left(\cos\frac{\pi x}{L}+1\right)-\frac{\Delta}{2}\left(1-\cos\frac{2\pi x}{L}\right) \tag{17}$$

In Eq.(17), x is the coordinate along the radial direction of the base plate, with origin ($x=0$) at the edge of the tank (i.e. at the wall-base plate junction) and w is the uplift height (at $x=0$). In addition, the second term in the right-hand side refers to the deflection of a fixed beam of rectangular cross-section with height $h=t_b$, width b and length L fixed at both of its ends and subjected to uniform distributed load $q=pb$ along its length (due to hydrostatic pressure p at the tank bottom), where Δ is the maximum value at mid-span. From structural mechanics, the value of Δ can be calculated from the hydrostatic pressure p as follows:

$$\Delta=\frac{1}{384}\frac{pbL^4}{EI} \tag{18}$$

or equivalently, after some algebraic manipulations

$$\Delta\simeq\frac{L}{35}\left(\frac{p}{E}\right)\left(\frac{L}{t_a}\right)^3 \tag{19}$$

where $EI = Ebt_a^3 \Big/ \left[12\left(1-v^2\right)\right]$ and t_a is the thickness of the annular plate. The two terms of Eq.(17) are also depicted in Figure 7.

Subsequently, the corresponding bending strain at the plate can be estimated from the bending curvature obtained from double differentiation of Eq.(17):

$$\varepsilon(x) = \frac{t_a}{2}\frac{d^2 w_1(x)}{dx^2} \tag{20}$$

Inserting Eq.(17) into Eq.(20) one obtains the following expression for the bending strain:

$$\varepsilon(x) = -\frac{\pi^2 t_a}{4L^2}\left(\mathrm{w}\cos\frac{\pi x}{L} + 4\Delta\cos\frac{2\pi x}{L}\right) \tag{21}$$

where the maximum strain occurs at $x = 0$ and is equal to:

$$\varepsilon_{\max} = \varepsilon(0) = \frac{\pi^2 t_a}{4L^2}(w + 4\Delta) \tag{22}$$

In the above equations, the uplifting length L should be considered as a function of uplifting size w, as indicated in Figure 12. Assuming the following expression of the uplifting length:

$$\frac{w}{D} = \beta^*\left(\frac{L}{D}\right)^4 \tag{23}$$

where β^* is a constant, one obtains:

$$\varepsilon(x) = \frac{\pi^2 L^2 t_a}{4}\left(\frac{\beta^*}{D^3}\cos\frac{\pi x}{L} + \frac{4p}{35Et^3}\cos\frac{2\pi x}{L}\right) \tag{24}$$

and the maximum strain is

$$\varepsilon_{\max} = \frac{\pi^2 t_a L^2}{4}\left(\frac{\beta^*}{D^3} + \frac{4p}{35Et_a^3}\right) \tag{25}$$

or, equivalently,

$$\varepsilon_{\max} = \frac{\pi^2}{4}\left(\frac{t_a}{L}\right)\left[\beta^*\left(\frac{L}{D}\right)^3 + \frac{4}{35}\left(\frac{p}{E}\right)\left(\frac{L}{t_a}\right)^3\right] \tag{26}$$

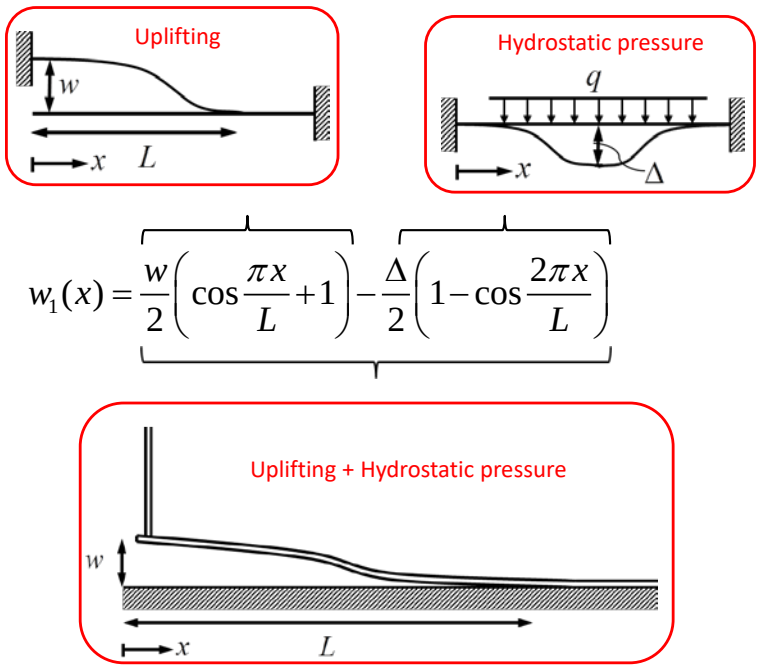

Figure 7: Schematic representation of the two terms of the assumed shape function of base plate deflection [Eq.(17)].

2.4 Local strain at weld toe

Equations (17)-(26) refer to "macroscopic" strains, which do not account for the local effects on the strain field due to weld discontinuity. Those effects can be accounted for through an appropriate "strain concentration factor" $SNCF$ that multiplies the strain values $\varepsilon(t)$ to obtain a reliable estimate of local strain $\overline{\varepsilon}(t)$ at the vicinity of the welded connection, which is suitable for fatigue analysis ($SNCF = \overline{\varepsilon}/\varepsilon$). In the case of strong cyclic loading, these strains are in the inelastic range of steel material, and therefore, an elastic analysis may not be appropriate for calculating the $SNCF$ value. In the present study, Stowell-Hardrath-Ohman method is employed for calculating the local inelastic strains at the weld toe [49]. According to this methodology, the local (hot spot) inelastic stress and

strain, denoted as $\overline{\sigma}$ and $\overline{\varepsilon}$ respectively, are related to the corresponding nominal values σ and ε through the following equation, written here according to the above notation:

$$SCF_{in} = \frac{SNCF}{SNCF - SCF + 1} \tag{27}$$

where SCF is the elastic stress concentration factor and SCF_{in} $(= \overline{\sigma}/\sigma)$ is the local stress concentration factor that includes inelastic effects.

To calculate the SCF value, a finite element model is necessary, as shown in Figure 8a. The finite element analysis focuses on the weld toe neighborhood ("hot spot" location), and therefore, the thickness of the annular base plate should be used for the base plate component in the finite element model. Furthermore, direct measurement of stress at the (Gauss) point nearest to the weld as obtained from the finite element analysis may not provide a reliable estimate of elastic stress concentration, due to sharp discontinuity of the stress/strain field at the weld toe. Therefore, an extrapolation of stresses to the weld toe from a defined region near the weld should be considered, as described in [50], and shown schematically in Figure 8b. The SCF value can be calculated as the ratio of the extrapolated stress at the weld toe over the nominal stress value, obtained from elementary structural mechanics.

Furthermore, to apply equation (27), a constitutive equation that relates stress and strain is required. Usually, a power-law equation for the cyclic stress-strain curve of the steel material is considered:

$$\sigma = K\varepsilon^n \tag{28}$$

This power-law relates both the nominal stress and strain σ and ε, as well as the local stress and strain $\overline{\sigma}$ and $\overline{\varepsilon}$, so that

$$\overline{\sigma} = K\overline{\varepsilon}^n \tag{29}$$

Given the nominal values σ and ε, related by equation (28), and the value of elastic SCF, the system of equations (27) and (29) can be solved for the two unknowns $\overline{\sigma}$ and $\overline{\varepsilon}$, and the $SNCF$ value is determined. The local strain values $\overline{\varepsilon}$ are used in the fatigue analysis described next.

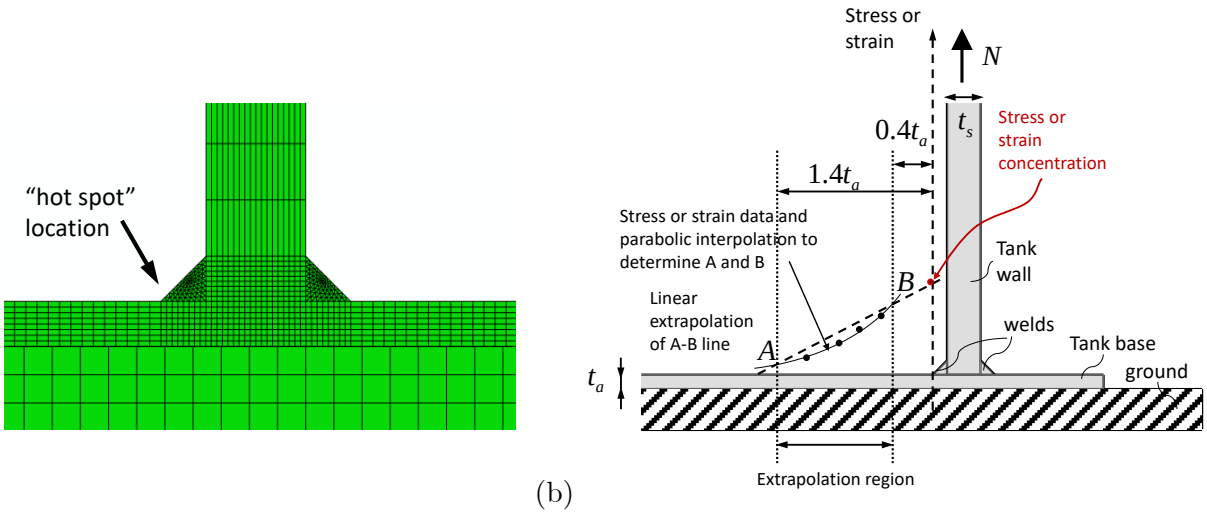

Figure 8: (a) Finite element model for calculating the elastic stress concentration factor SCF; (b) schematic representation of the extrapolation method to calculate SCF.

2.5 Fatigue analysis

The time history of bending strains $\overline{\varepsilon}$ from seismic action is an irregular function. Therefore, the "rainflow cycle counting" method is employed to obtain a loading spectrum, which expresses the applied strain ranges $\Delta\varepsilon_i$ and the corresponding numbers of cycles for each range, n_i. Furthermore, in order to determine tank failure due to fatigue, an appropriate fatigue curve is necessary which provides the number of cycles to failure N_i for each strain range $\Delta\varepsilon_i$. Finally, the values of n_i, N_i are combined to provide a fatigue damage parameter D calculated through Miner's rule:

$$D = \sum_i \frac{n_i}{N_i} \tag{30}$$

where fatigue failure is assumed to correspond to a unit value.

3. RESULTS

3.1 Description of Case Studies

Two typical fixed-roof liquid storage tanks are considered and analyzed in the present study. They represent real cases, i.e. tanks constructed in areas of seismic activity. The tanks have been designed using the relevant API 650 rules, before the issue of the new version of Appendix E, in 2007 [51].

The first tank is a moderately-broad unanchored tank, referred to as Tank I. It is a 27.8-meter-diameter tank with a total height of 16.5 meters. The filling height of the tank H is equal to 15.7, which corresponds to an aspect ratio of the tank, $\gamma\left(=H/R\right)$ equal to 1.131. The tank thickness varies from 6.4 mm at its top course to 17.7 mm at its bottom course, and the bottom plate is 6 mm thick with an 8-mm-thick annular plate. It has an L120×120×12 stiffening ring at the top (wind stiffener) and the mass of the roof and the tank shell are 35,000 kg and 118,100 kg, respectively.

The second tank, referred to as Tank II, is a broad 46.9-meter-diameter unanchored tank with a total height of 19.95 meters. The filling height of the tank H is equal to 18.37 resulting in an aspect ratio, $\gamma\left(=H/R\right)$ equal to 0.783. The tank thickness varies from 8 mm at its top course to 22.23 mm at its bottom course. It has an L76×76×10 stiffening ring at its top, whereas the mass of the roof and tank shell are 45,863.5 kg and 301,549 kg, respectively.

In both tanks, the contained liquid is assumed to be water ($\rho=1000$ kg/m^3) and the material of the tank shell, the bottom plate and the roof is structural steel S235 (equivalent to A36 steel) with yield stress $\sigma_y=235$ MPa. Despite the fact that those tanks have been constructed as unanchored, for the purposes of the present study, they are simulated as both anchored and unanchored. Both tanks have fixed truss roofs consisting of meridional and parallel L and UPN beams. The tank geometries are depicted in Figure 9.

3.2 Static Analysis Results

Representative results from the seismic response of the two tanks with unanchored conditions are reported in the present section, as obtained from the finite element static analysis model.

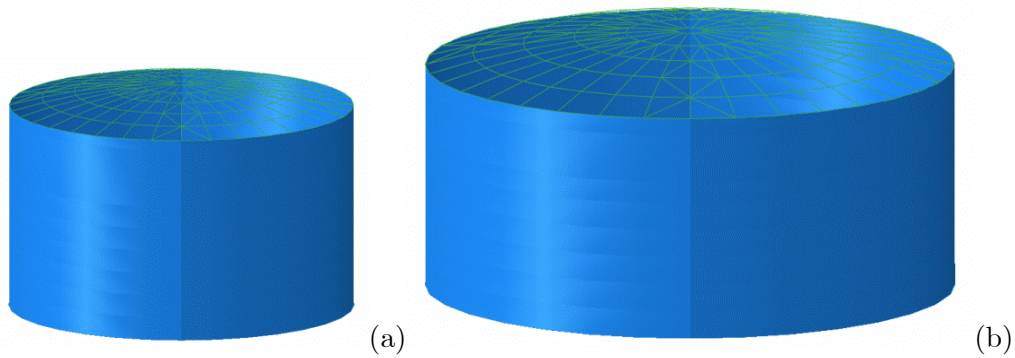

(a) (b)

Figure 9: Tanks used for the present numerical study; (a) Tank I, (b) Tank II.

The evolution of top horizontal displacement of the two tanks is shown in Figure 10, in terms of the overturning moment M due to hydrodynamic loading. The maximum overturning moment is computed as the sum of the overturning impulsive and convective moments, at each time increment of the analysis. The value of u is normalized by the liquid height H and the value of M is normalized by WH, where W is the total weight of the contained liquid, a normalization scheme also suggested in EN 1998-4 [26]. At the level of normalized overturning moment equal to 0.03, the slope of the curve changes significantly, indicating the beginning of uplifting for both tanks, and the occurrence of substantial local inelastic deformation. Furthermore, the results indicate a smaller sensitivity of the uplifting on the value of tank aspect ratio (H / R), than the one suggested in EN 1998-4.

The global behaviour of the tanks is also represented in Figure 11, which shows the maximum vertical uplift of the simulated unanchored tanks in terms of the normalized overturning moment at the tank base. The dotted curves for aspect ratio $\gamma = H / R =$ 0.8, 1.0, 2.0 have been reported in EN 1998-4 as obtained from the work of Scharf [52]. The comparison between the present finite element results and

those in EN 1998-4 also shows that the Scharf curves can be non-conservative, predicting smaller uplift than the ones obtained herein, using more advanced and detailed finite element modeling.

For estimating the radial bending stresses within the plate, the calculation of length L of the uplifted part of the tank bottom is necessary. The relationship between the length of the uplifted part of the base (normalized by R, the tank radius) and the overturning moment (normalized by WH, where W is the weight of the tank liquid containment) is shown in Figure 12. The results indicate that the value of the length of the uplifted base plate is an increasing function of the value of the overturning moment.

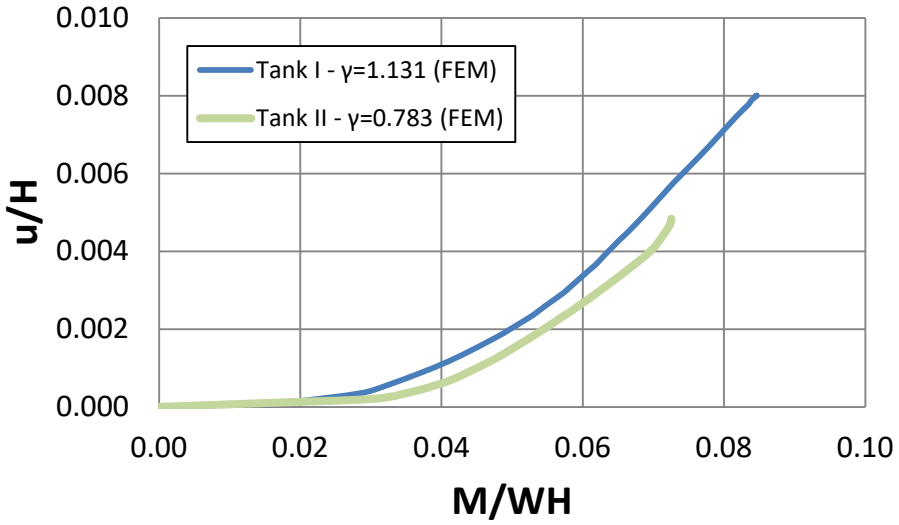

Figure 10: Normalized overturning moment M versus normalized top horizontal displacement u, as obtained from the present finite element static analysis.

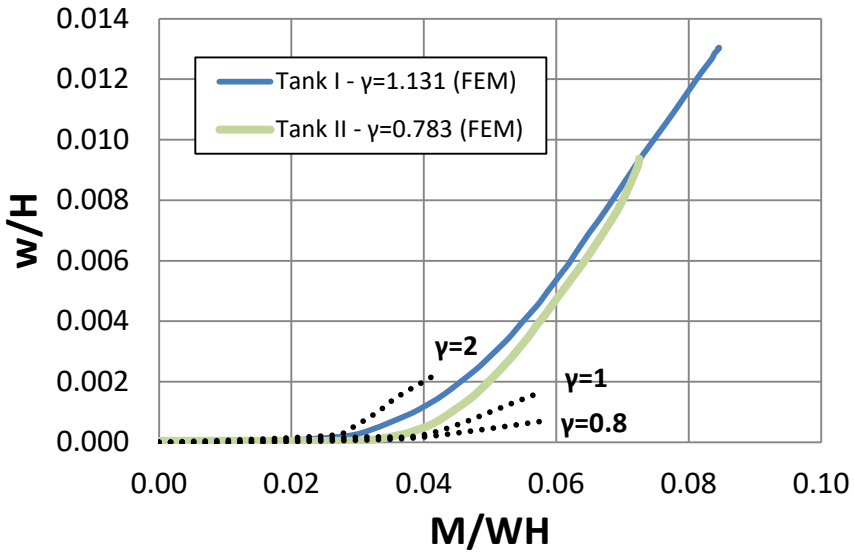

Figure 11: Maximum normalized vertical uplift of the tank w versus normalized overturning moment M ; the present finite element results are compared with the corresponding curves reported in EN 1998-4 [26].

Combining the results from Figure 10 and Figure 11 one can develop the graph of Figure 12. It is interesting to note that upon occurrence of uplifting, the dependence of L on the vertical uplift w is quasi linear. Comparison of the present numerical results with those included in paragraph A.9 of EN 1998-4 [26], initially reported by Scharf [52], shows that the Scharf curves indicate a similar trend in uplifting behaviour, but they are somewhat conservative. Normalization of the parameters of Figure 13 produces Figure 14, which gives the relationship between the vertical uplift and uplifted length of the tank in a more universal manner.

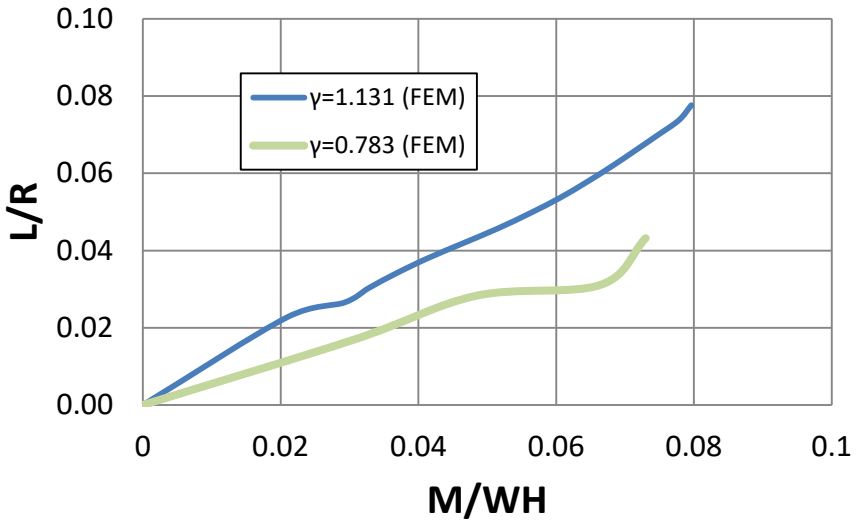

Figure 12: Normalized length of the uplifted part of tank base plate as a function of the normalized overturning moment.

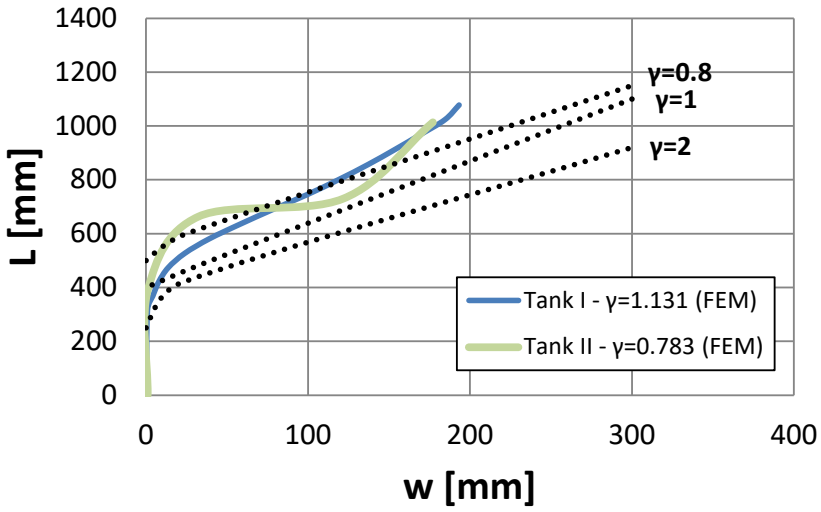

Figure 13: Length of uplifted part of the base as a function of the vertical uplift at the edge; the present finite element results are compared with the corresponding curves reported in EN 1998-4 [26].

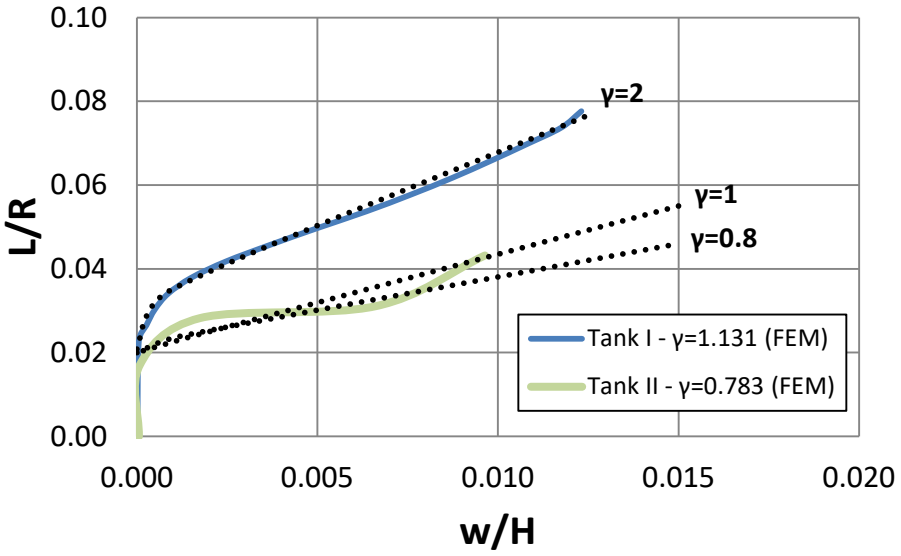

Figure 14: Normalized length of uplifted part of the base as a function of the normalized vertical uplift at the edge; the present finite element results are compared with the corresponding curves reported in EN 1998-4 [26].

The evolution of membrane forces with increasing overturning moment, at the uplifting side of the tank, is depicted in Figure 16 for both anchored and unanchored tanks. These graphs are also compared with the analytical formula of Eq.(31):

$$N = \frac{1.273M}{D^2} - w_t \tag{31}$$

where M is the overturning moment, R is the radius of the tank, and w_t is the load per unit circumferential length because of shell and roof dead weight acting at the base of tank shell.

Overall, the comparison of the membrane force values obtained numerically and the predictions from the simple analytical formula shows a fair overall agreement (Figure 16). This indicates that the analytical formula can be used for obtaining reasonable estimates of the maximum force, in the course of a simplified dynamic analysis.

The relationship of the overturning moment M and the "rocking" angle ψ is shown in Figure 17 and Figure 18 for the two tanks under consideration. In these graphs, ψ is defined as the average rotation of the tank base due to uplifting (rocking angle), calculated by the following equation, and expressed schematically in Figure 15:

$$\psi = \frac{w}{D} \tag{32}$$

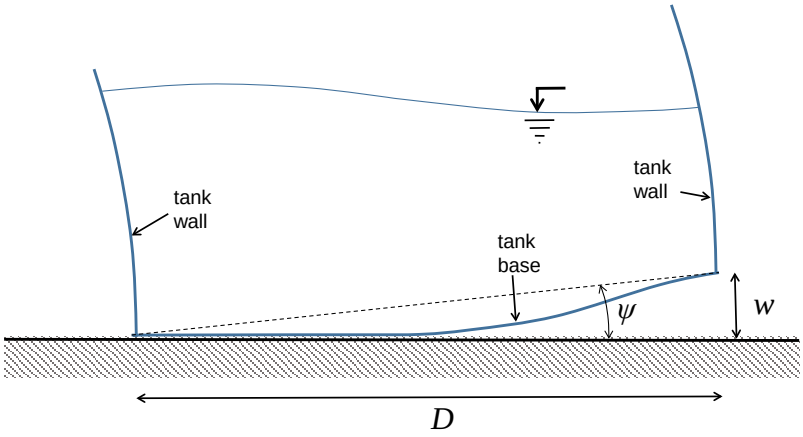

Figure 15: Definition of uplifting angle ψ.

The results in Figure 17 and Figure 18 show that the $M-\psi$ relationship can be approximated with a bilinear expression also plotted in the same graphs. The $M-\psi$ expressions shown in the graphs are used in the simplified dynamic analysis for the $M(\psi)$ function. This function is considered symmetric for the case of negative values of uplifting angle ψ. It is also noticed that unloading follows the same path, so that the uplifting spring is modeled as a nonlinear elastic component, an assumption also adopted in relevant works [10] [29]. The equivalent plastic strain developed at the tank base plate is shown in Figure 19(a) and Figure 20(a) for Tank I and II respectively, in terms of the horizontal coordinate x. The equivalent plastic strain becomes maximum at two locations of the base plate, (a) at the junction of the tank wall and the base plate and (b) at a small distance from the weld where change

of slope occurs. At these two locations significant plastic yielding develops. These locations are depicted in Figure 19(b) and Figure 20(b), for Tank I and II respectively, at various uplifting configurations.

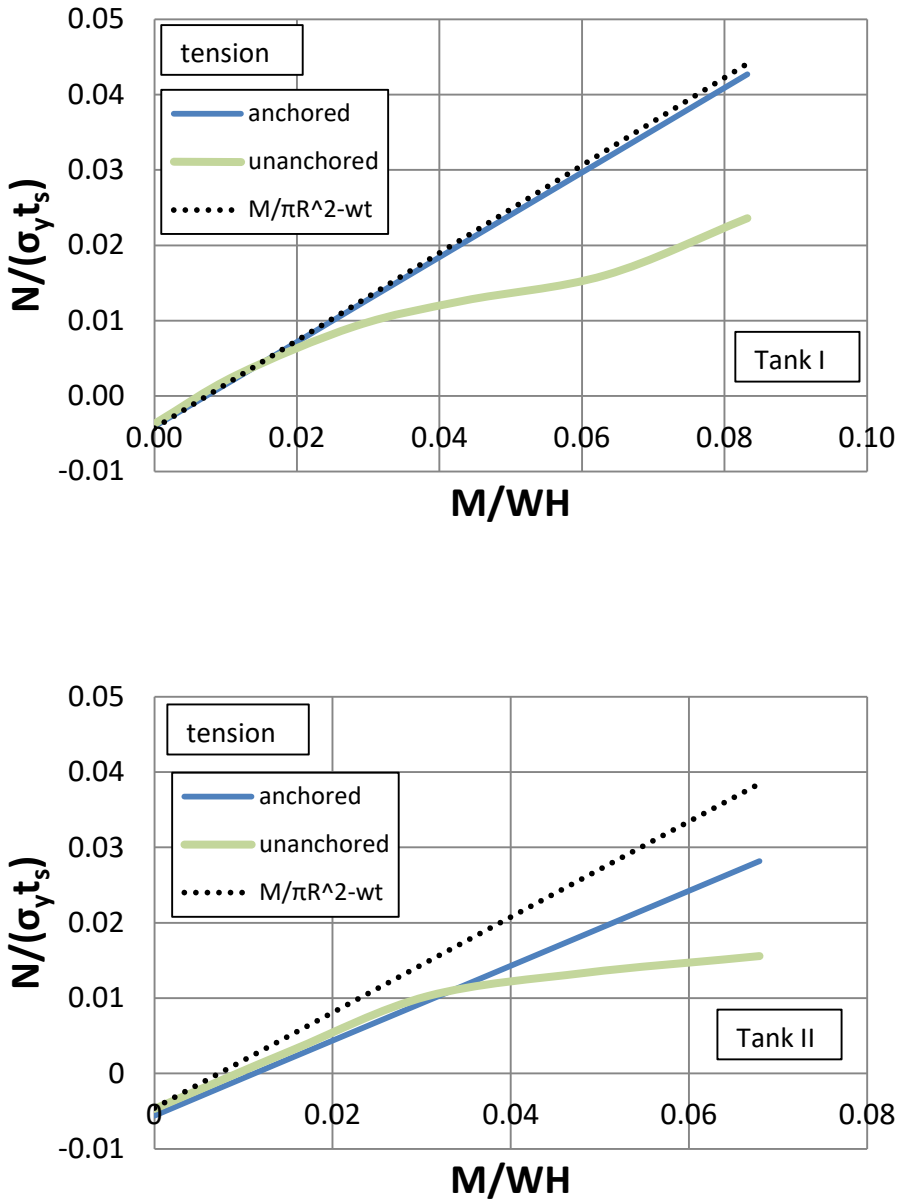

Figure 16: Membrane uplifting forces for anchored and unanchored Tanks I and II in terms of the overturning moment; comparison of numerical results with the analytical formula.

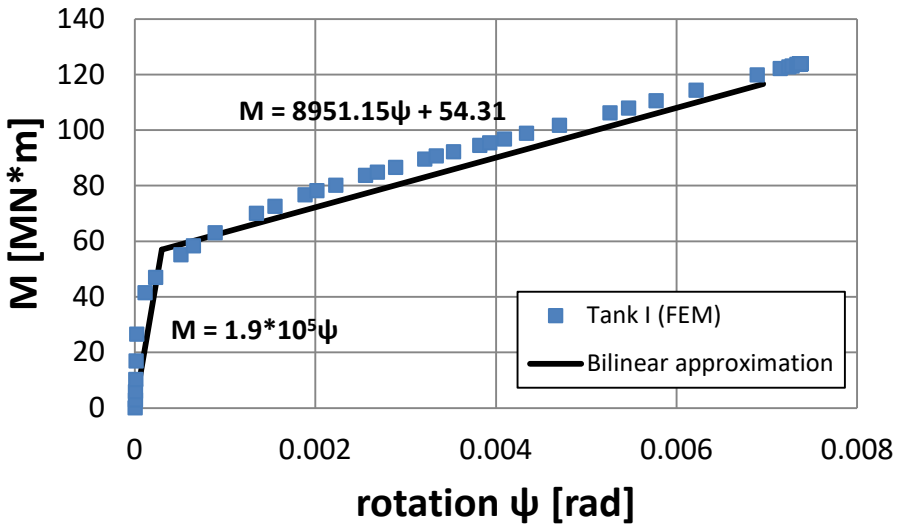

Figure 17: Overturning moment versus base rotation subjected to lateral load static analysis (Tank I).

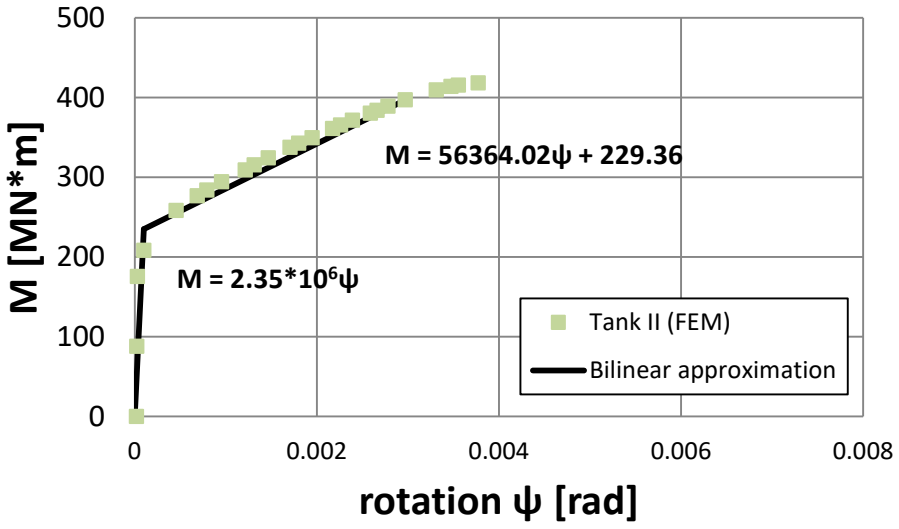

Figure 18: Overturning moment versus base rotation subjected to lateral load static analysis (Tank II).

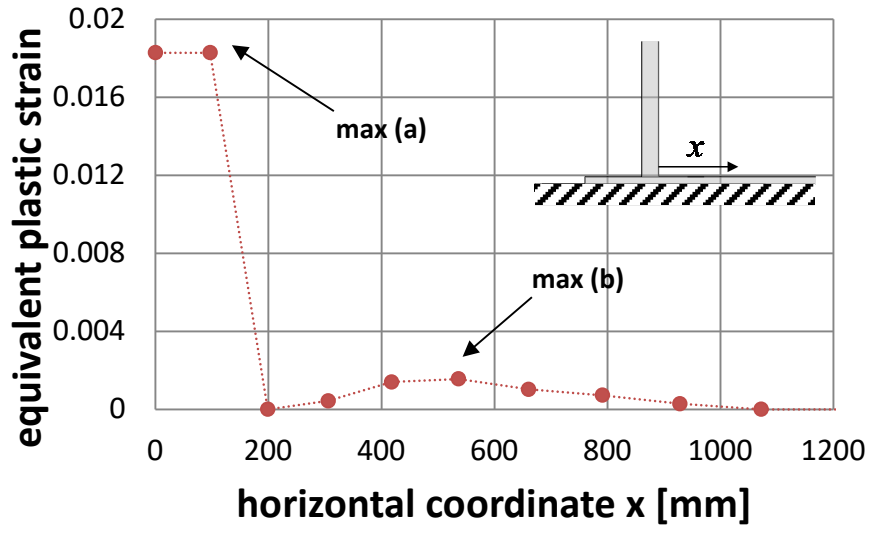

(a)

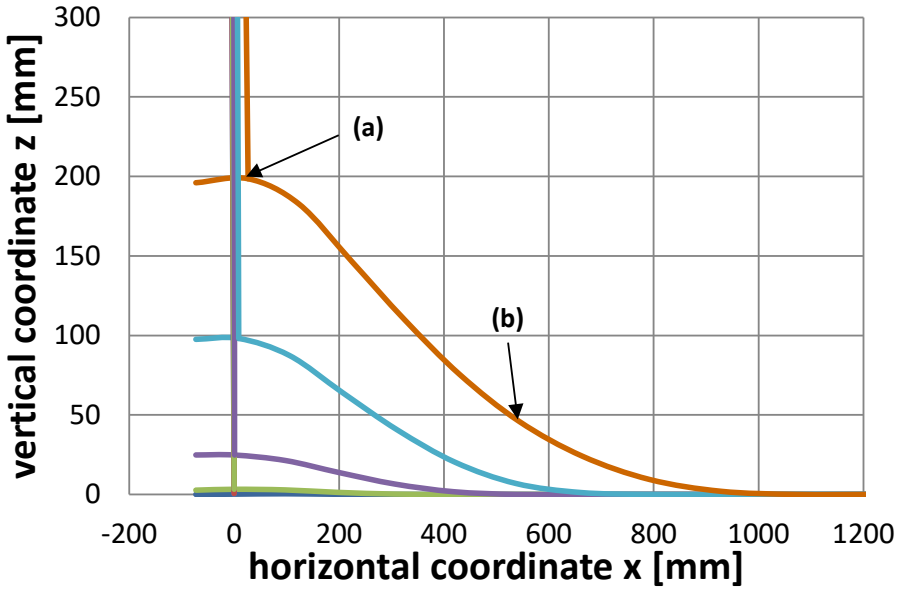

(b)

Figure 19: (a) Equivalent plastic strain at the nodes of the tank base plate in terms of the horizontal coordinate x for Tank I, on the inner surface of the base plate at 0.106g; (b) Deformed bottom plate of Tank I; the arrows (↓) show the two points of maximum equivalent plastic strain.

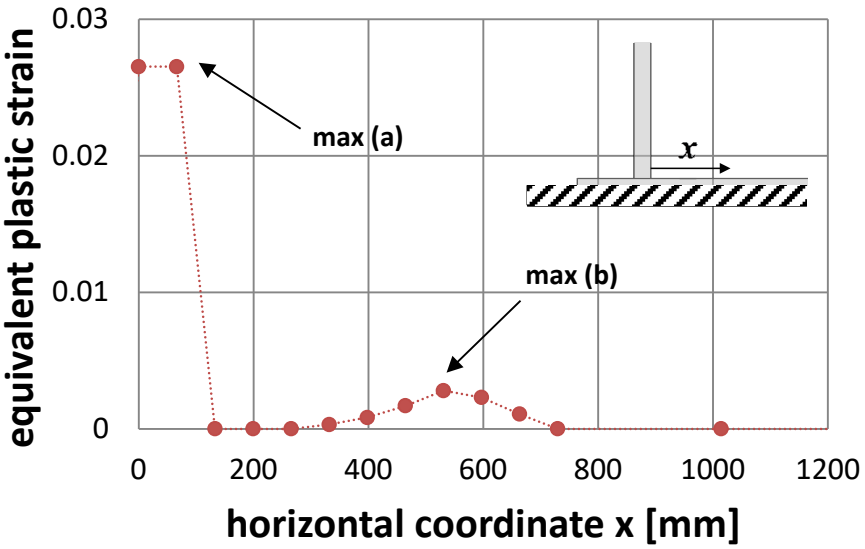

(a)

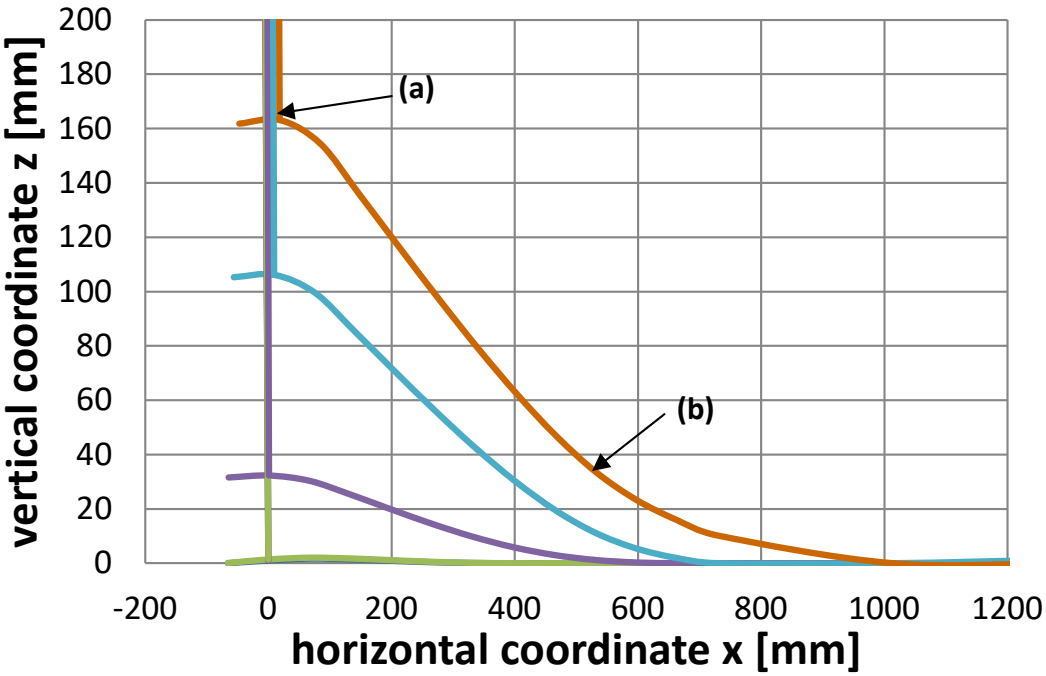

(b)

Figure 20: (a) Equivalent plastic strain at the nodes of the tank base plate in terms of the horizontal coordinate x for Tank II, on the inner surface of the base plate at 0.119g; (b) Deformed bottom plate of Tank II; the arrows (↓) show the two points of maximum equivalent plastic strain.

3.3 Dynamic Analysis Results

Using the simplified dynamic model described in the previous section, Tanks I and II have been analyzed dynamically. The Düzce earthquake (Düzce, Turkey, 1999), with a peak ground acceleration PGA equal to 0.36 g, is employed as the seismic input of the seismic analyses, as shown in Figure 21. The two tanks have been analyzed under both anchored and unanchored conditions.

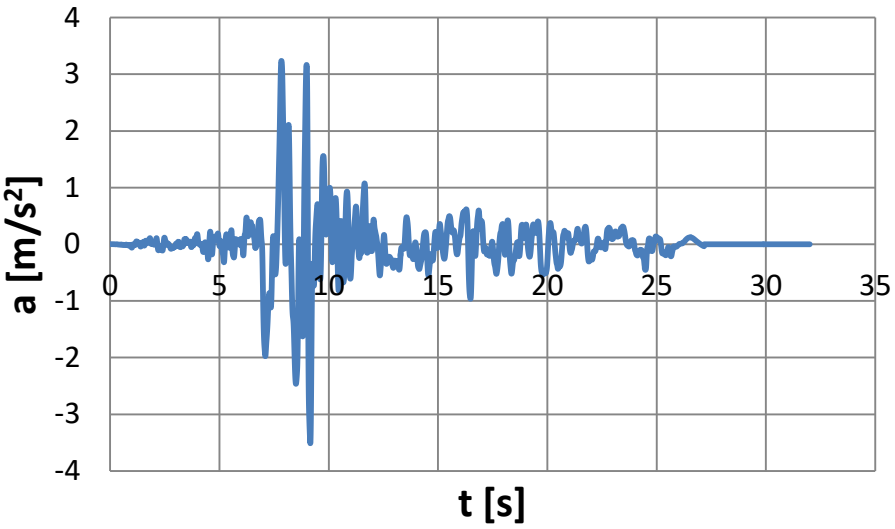

Figure 21: Accelerogram of the Düzce earthquake, Turkey (1999).

In Figure 22 the time history of the base moment M is shown for Tank I and Tank II respectively, under anchored conditions. Furthermore, Figure 23 and Figure 24 refer to the time history of the vertical uplift w, at the two sides (right and left) of Tank I and Tank II respectively, under unanchored conditions. In the present case, the damping ratios, ξ_I and ξ_O, are chosen equal to 5% and 10% respectively. The 5% value for ξ_I is typical for steel structural systems subjected to seismic loading, also suggested in [26]. On the other hand, there is no evidence for the value of ξ_O; the 10% value for ξ_O is a rather high value, which has been chosen by the authors to account for the significant energy dissipation expected during repeated uplifting of the tank. The time history of the overturning base moment M for the two tanks under unanchored conditions is also shown in Figure 25.

Using the relation between the uplifting length L and the uplifting displacement w in equation (23), with β^* found equal to 1.114×10^{-5} for Tank I and 2.233×10^{-6} for Tank II, the strain histories at the right and left side of the two tanks are computed for the earthquake loading under consideration, as shown in Figure 27 and Figure 28 for Tank I and Tank II respectively.

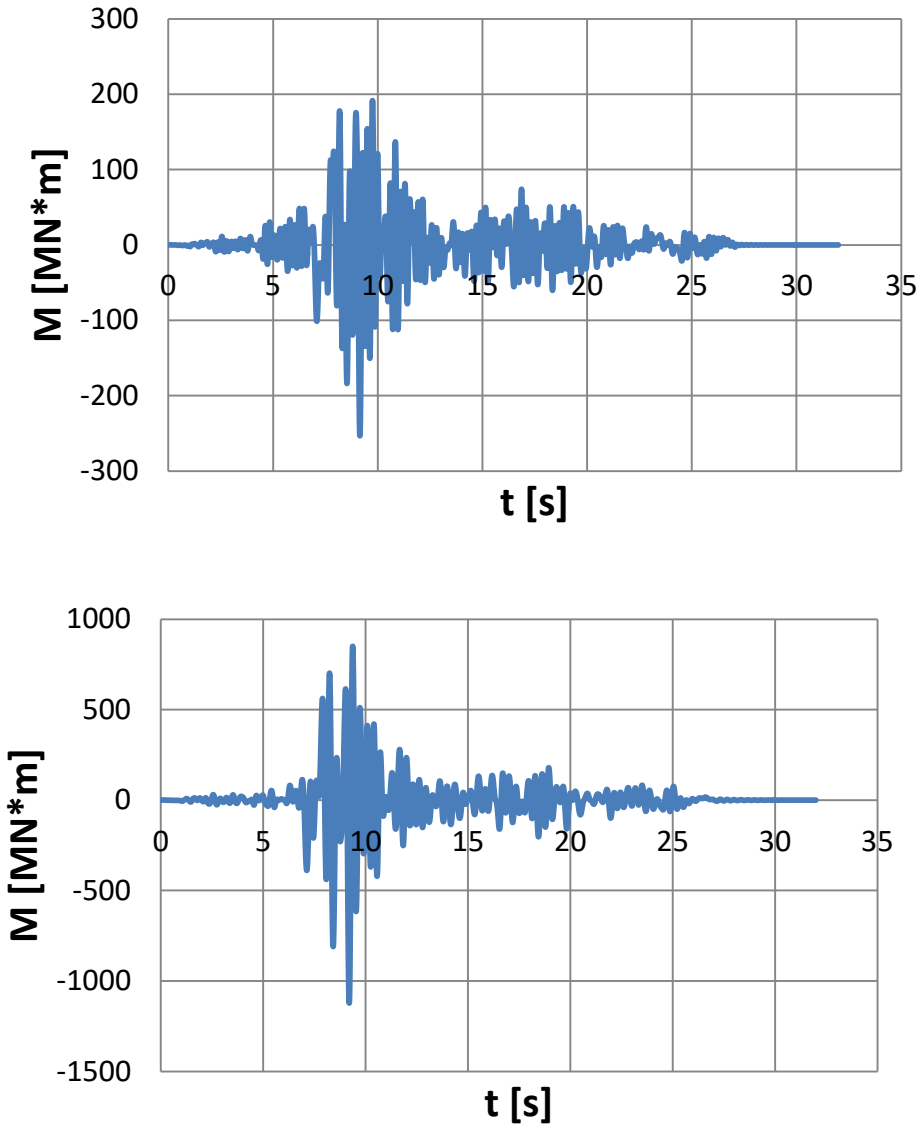

Figure 22: Time history of the base moment M for anchored Tank I and Tank II subjected to Düzce 1999 seismic action.

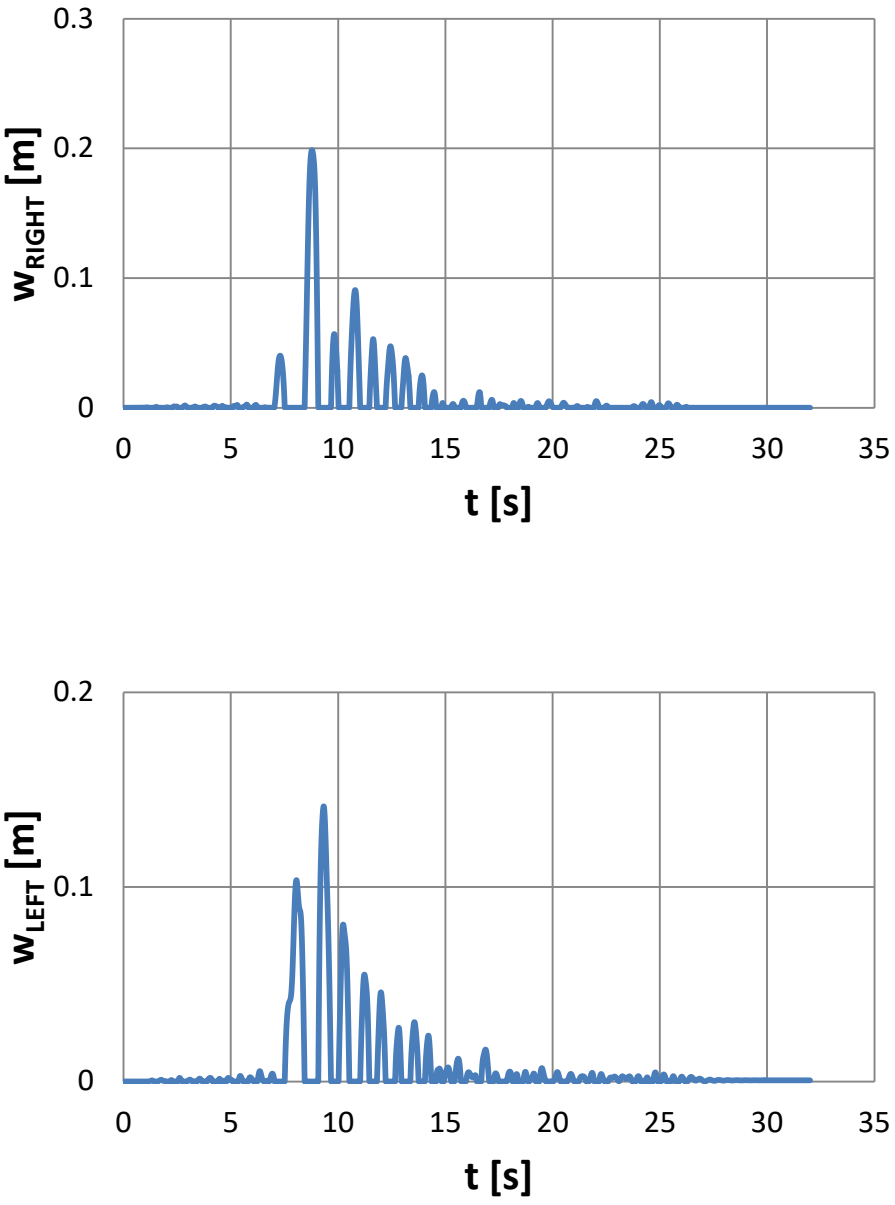

Figure 23: Time history of vertical uplift w at the right and left side of unanchored Tank I.

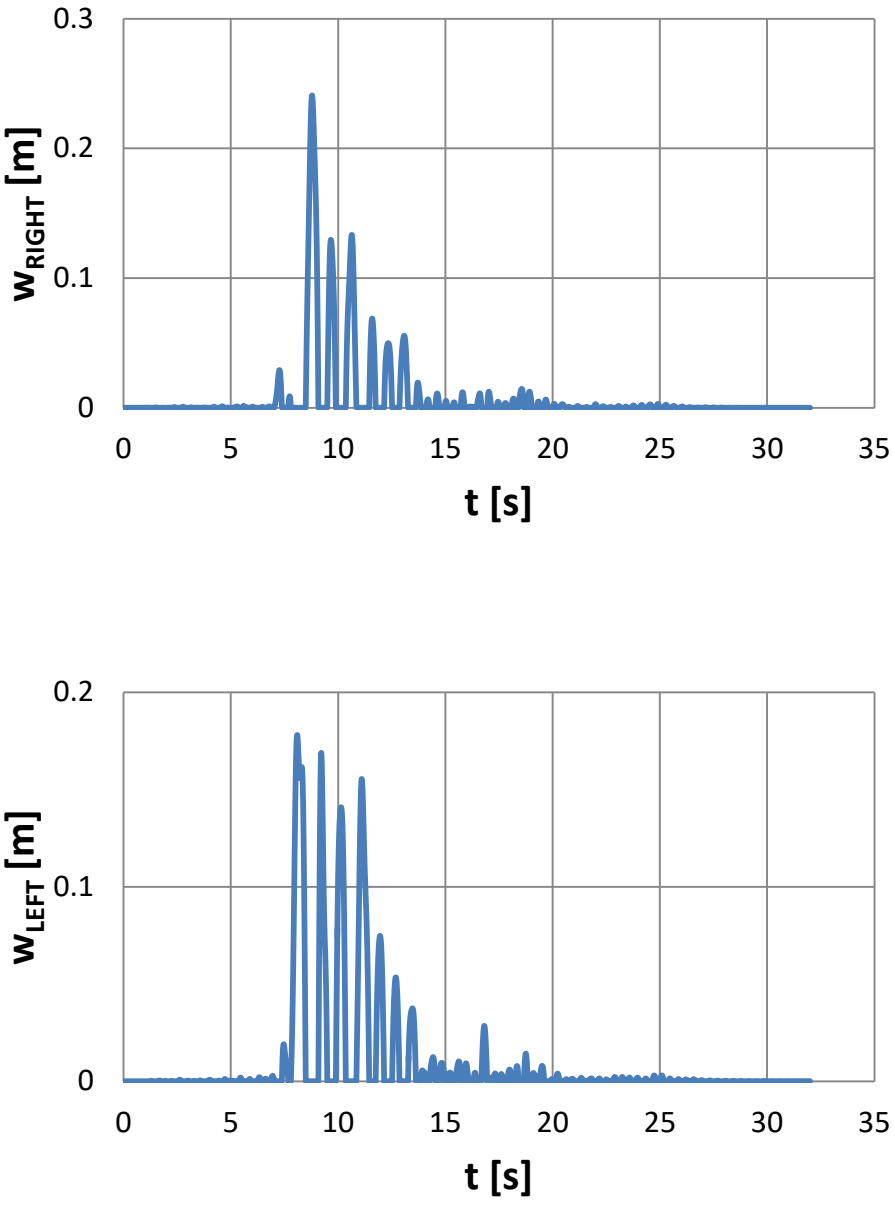

Figure 24: Time history of vertical uplift w at the right and left side of unanchored Tank II.

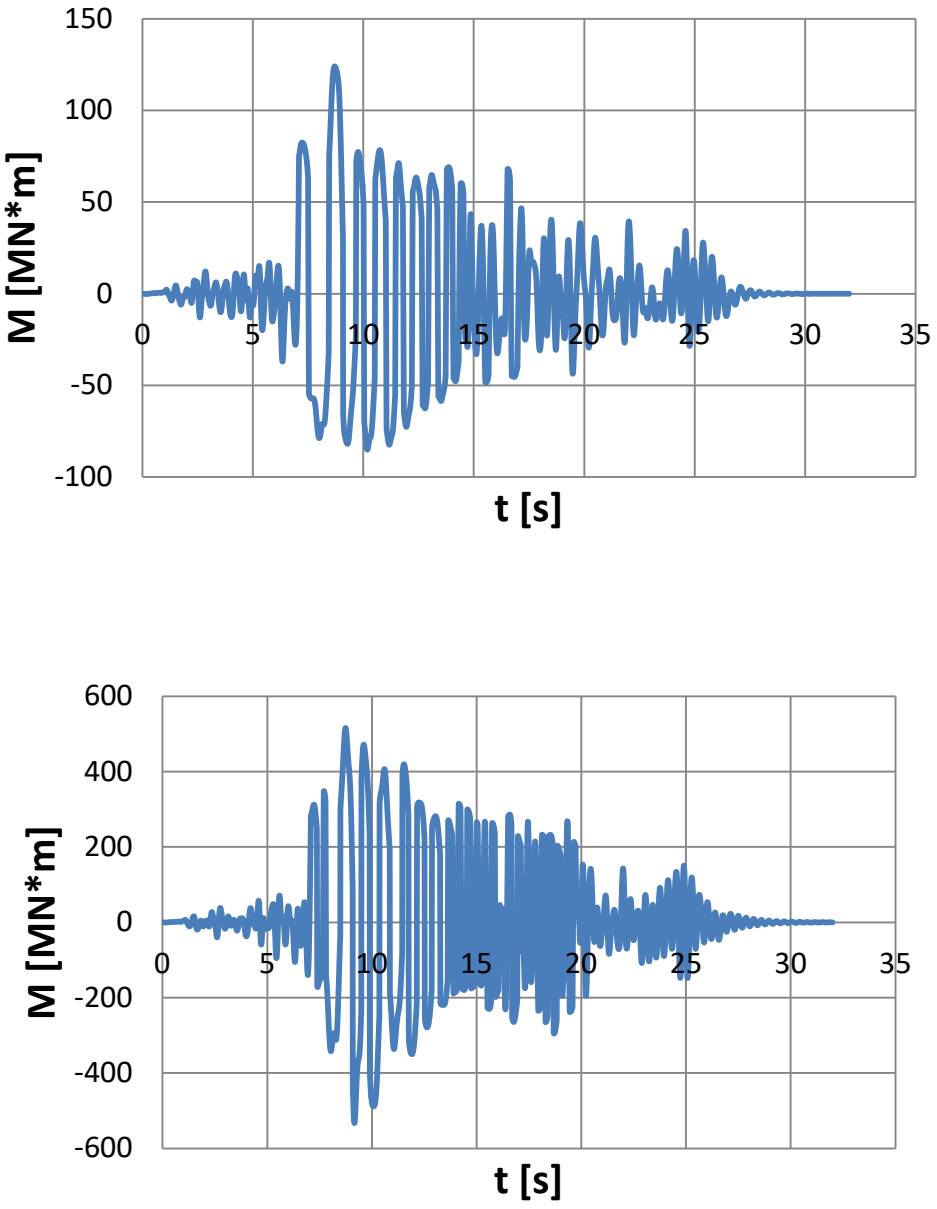

Figure 25: Time history of base moment M for unanchored Tanks I and II.

To conduct a fatigue analysis of the base plate connection, the $SNCF$ value is calculated through the value of the elastic SCF and the use of Eq. (27). Considering an axisymmetric finite element model of the welded connection area, as described in the previous section, and using the extrapolation method

suggested in [50], the elastic SCF value is found equal to 1.32 for Tank I and 1.23 for Tank II. In addition, the parameters of power-law stress-strain equation for typical steel material behavior are taken equal to $K = 679$ MPa (98.4 ksi) and $n = 0.10$ [53] (which is a conservative value), resulting in $SNCF$ values for the two tanks equal to 3 and 2.6 respectively.

In the present study, the linear $\log \Delta\varepsilon - \log N$ fatigue curve shown in Figure 26 is used. This fatigue curve for values of cycles N greater than 10^5 cycles ($\log N > 5$), i.e. high-cycle fatigue, coincides with the mean curve of BS 7608 [54], for Tee joint plated welded detail of Class F2 (see Table 8 of BS 7608). For smaller numbers of loading cycles, which are of most interest to our case, the log-log line is extended linearly into the low-cycle fatigue regime. It should also be noted that the left end of the curve ($N = 1$) indicates $\Delta\varepsilon = 5\%$ which corresponds to static (monotonic) loading conditions, a reasonable value for strain limit under monotonic loading. It should be noted that alternatively, instead of using the simple curve of Figure 26, one may use a more elaborate low-cycle fatigue curve (e.g. Coffin-Manson curve), provided that adequate information on the mechanical behavior of tank material is available.

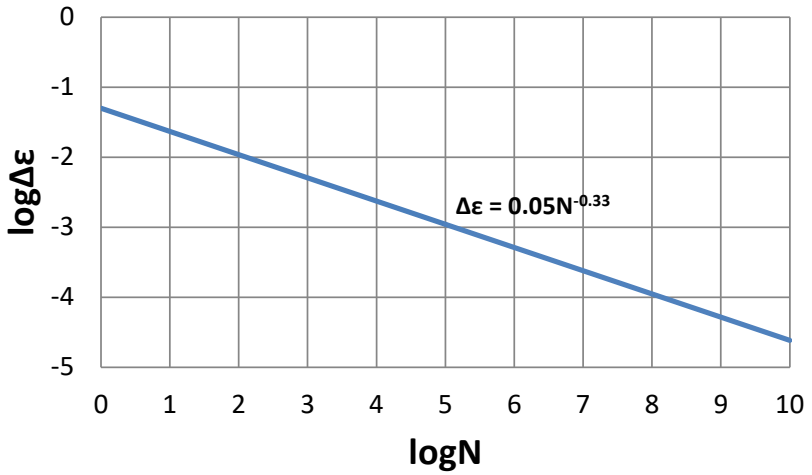

Figure 26: Strain amplitude fatigue curve used in the present study plotted in a log-log scale.

Using the time history of strain in Figure 27 and Figure 28, the strain ranges $\Delta\varepsilon_i$ and the corresponding number of acting cycles n_i as obtained from the rainflow counting method are shown in Table 1 and Table 2 for the two tanks under consideration. Furthermore, the number of cycles to failure N_i corresponding to $\Delta\varepsilon_i$ obtained from the fatigue curve of Figure 26 and together with the results for the fatigue damage factor, obtained from Miner's rule, are also shown in Table 1 and Table 2. For the seismic input considered, the value of damage parameter D can be equal to 20%, which corresponds to a significant part of total fatigue resistance.

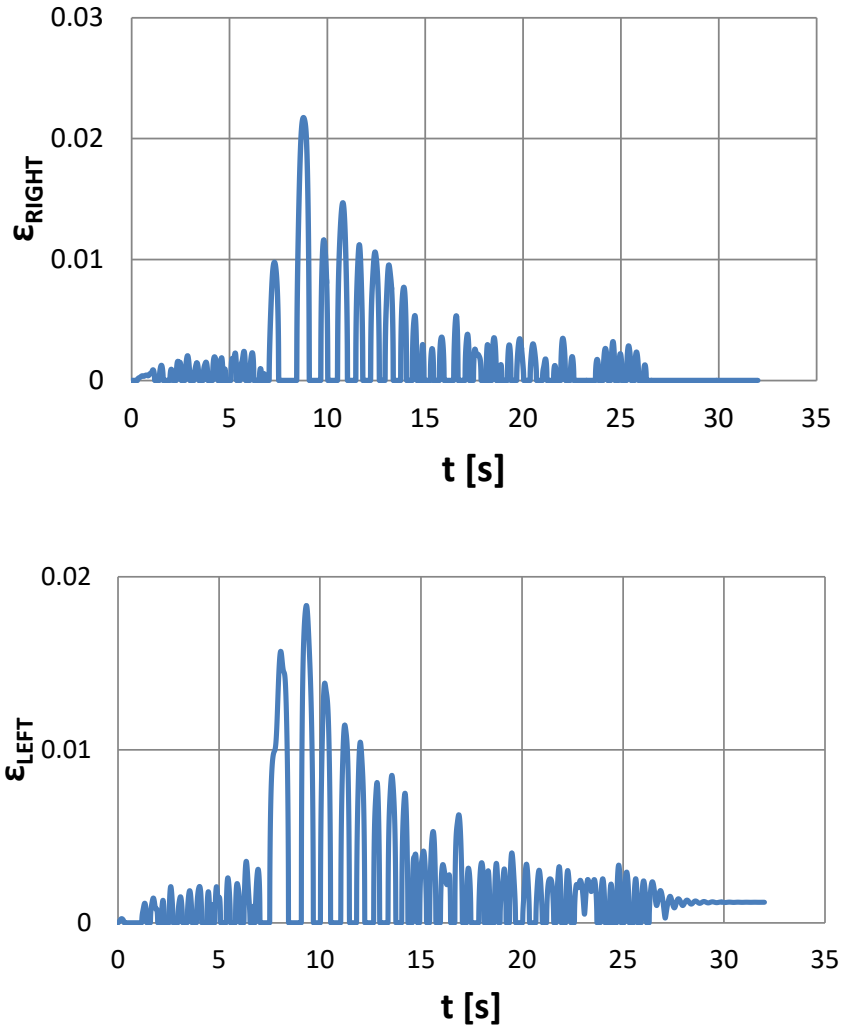

Figure 27: Time history of the local bending strains at the plate-shell connection at the right and left side of Tank I for the seismic input of Figure 21.

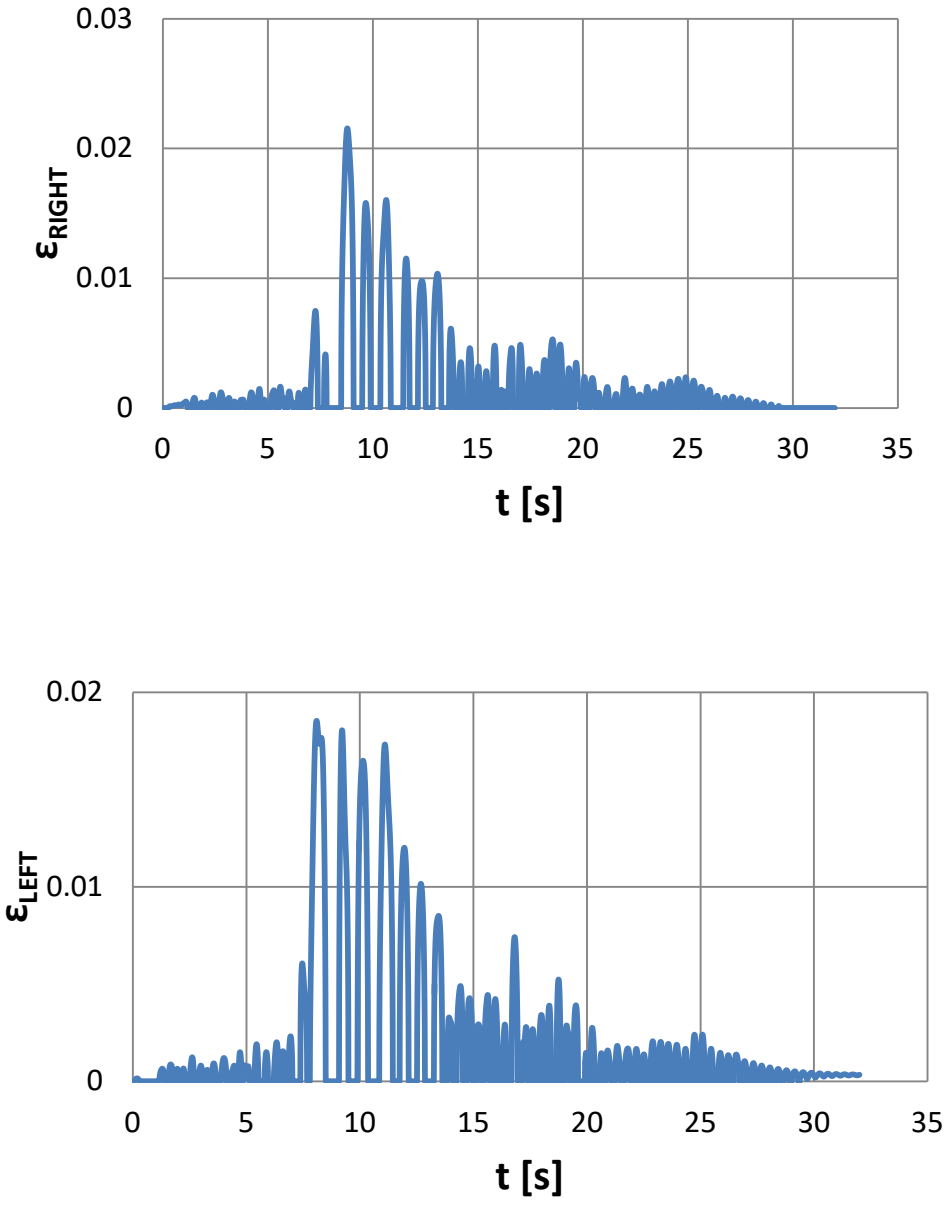

Figure 28: Time history of the local bending strains at the plate-shell connection at the right and left side of Tank II for the seismic input of Figure 21.

Table 1: Fatigue analysis of Tank I using rainflow cycle counting method.

Right Side of Tank I				Left Side of Tank I			
$\Delta\varepsilon$	$\Delta\overline{\varepsilon}$	n_I	N_I	$\Delta\varepsilon$	$\Delta\overline{\varepsilon}$	n_I	N_I
0.0003	0.0009	19	162479	0.0003	0.0008	25	295220
0.0009	0.0027	22	6335	0.0008	0.0023	19	10871
0.0015	0.0046	3	1376	0.0013	0.0038	13	2333
0.0021	0.0064	0	502	0.0018	0.0054	1	846
0.0027	0.0082	1	236	0.0023	0.0069	2	397
0.0033	0.0100	3	130	0.0028	0.0084	2	217
0.0039	0.0118	2	79	0.0033	0.0099	1	131
0.0045	0.0136	0	51	0.0038	0.0115	1	85
0.0051	0.0154	1	35	0.0043	0.0130	0	59
0.0057	0.0172	0	25	0.0048	0.0145	1	42
0.0063	0.0190	0	19	0.0053	0.0160	1	31
0.0069	0.0208	1	14	0.0059	0.0176	1	24
$D = 0.158$				$D = 0.140$			

Table 2: Fatigue analysis of Tank II using rainflow cycle counting method.

Right Side of Tank II				Left Side of Tank II			
$\Delta\varepsilon$	$\Delta\overline{\varepsilon}$	n_I	N_I	$\Delta\varepsilon$	$\Delta\overline{\varepsilon}$	n_I	N_I
0.0003	0.0009	44	181345	0.0003	0.0008	39	260992
0.0010	0.0027	15	6671	0.0009	0.0023	21	10237
0.0017	0.0045	8	1432	0.0015	0.0039	7	2225
0.0024	0.0063	1	520	0.0021	0.0054	3	812
0.0031	0.0081	1	244	0.0027	0.0070	1	382
0.0038	0.0099	2	133	0.0033	0.0085	1	209
0.0045	0.0117	1	81	0.0039	0.0101	1	127
0.0052	0.0135	0	53	0.0045	0.0116	1	83
0.0059	0.0153	2	36	0.0051	0.0131	0	57
0.0066	0.0171	0	26	0.0056	0.0147	0	41
0.0073	0.0189	0	19	0.0062	0.0162	1	30
0.0079	0.0207	1	15	0.0068	0.0178	3	23
$D = 0.164$				$D = 0.200$			

3.4 A note on the effect of roof stiffness on uplifting

An interesting issue on unanchored tanks refers to the effect of tank roof on uplifting behavior. For the purpose of examining this effect, a numerical study has been performed using finite element models of unanchored tanks with different aspect ratios, considering nonlinear static analysis, as described in section 3.2. The tanks have been modeled with and without a truss (fixed) roof, and their geometric characteristics are summarized in Table 3. For the tanks without a truss roof, an L-shape stiffening ring has been considered at the top circular section of the cylinder, referred to as "wind stiffeners"; the dimensions of the "wind stiffeners" were chosen according to the relevant provisions of Paragraph 5.9.6 of API 650 standard [51]. All tanks have a total height of 12 m, a filling height of 10 m, whereas the diameter of the tanks ranges from 10 to 32 m, corresponding to aspect ratios ($\gamma = H / R$) ranging between 0.625 and 2. The tank shell thickness has been designed according to the relevant provisions of API 650 [51]. The contained liquid is assumed to be water ($\rho = 1000$ kg/m^3) and the material of the tank shell, the bottom plate and the roof is structural steel grade S235 (equivalent to A36 steel) with yield stress σ_y = 235 MPa.

The results of this numerical study are shown in Figure 29 and demonstrate that the stiffness provided by the roof against ovalization of the tank top cross-section may have a substantial effect on the uplifting size of the tank. More specifically, the presence of a fixed roof leads to a decrease of the vertical uplift of the tanks, as shown in Figure 30 and Figure 31, which depict representative finite element results of the tanks under consideration. The results indicate that for a value of applied normalized moment M/WH equal to 0.05, the tanks with a fixed roof exhibit a 70% smaller uplift.

Table 3: Characteristics of the tanks used in the parametric study.

	D [m]	H [m]	H_T [m]	$\gamma = H / R$	t_1 [mm]	t_2 [mm]	t_3 [mm]	t_b [mm]
Tank 1	10	10	12	2	6	5	5	6
Tank 2	11	10	12	1.818	6	5	5	6
Tank 3	12.4	10	12	1.613	6	5	5	6
Tank 4	13	10	12	1.538	6	5	5	6
Tank 5	14	10	12	1.43	6	5	5	6
Tank 6	20	10	12	1	7.5	6	6	7
Tank 7	26	10	12	0.77	9.6	7	6	9
Tank 8	32	10	12	0.625	12	8	6	11

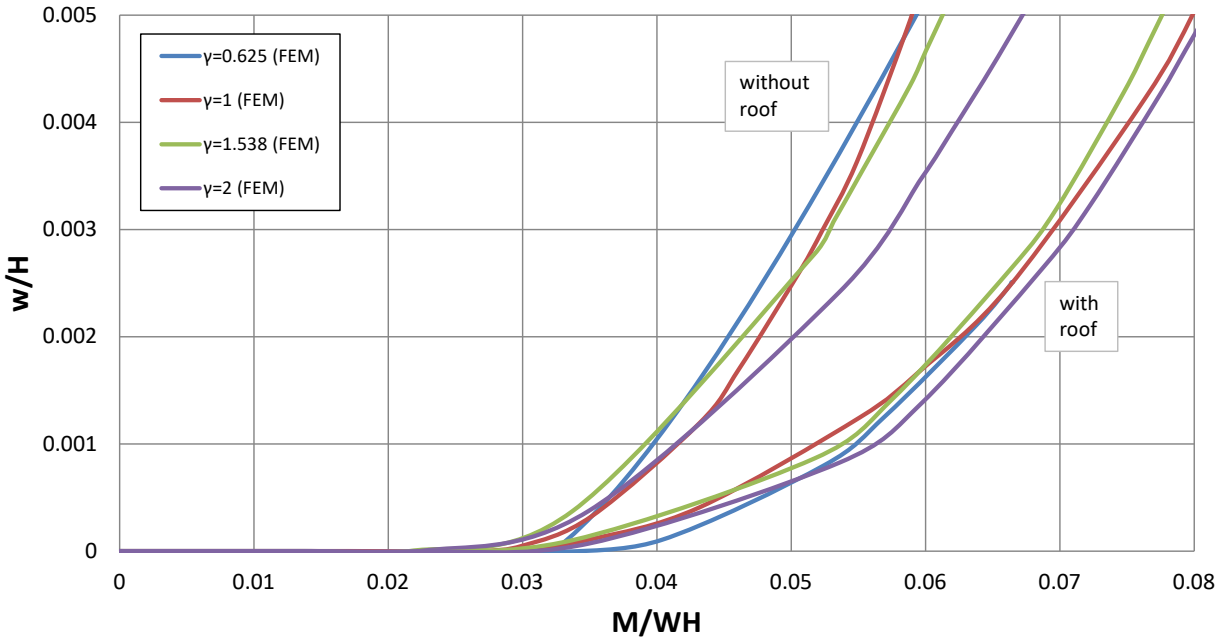

Figure 29: Results of numerical study for unanchored tanks with different aspect ratios, modeled with and without a roof.

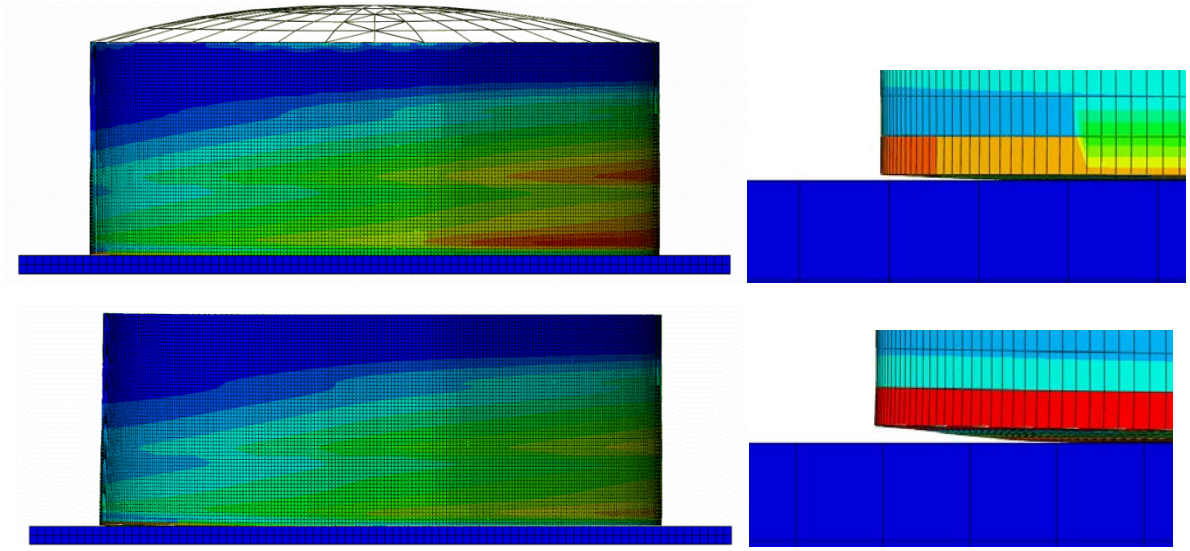

Figure 30: Finite element modeling of the tank with aspect ratio equal to 0.625; (a) with roof, (b) without roof.

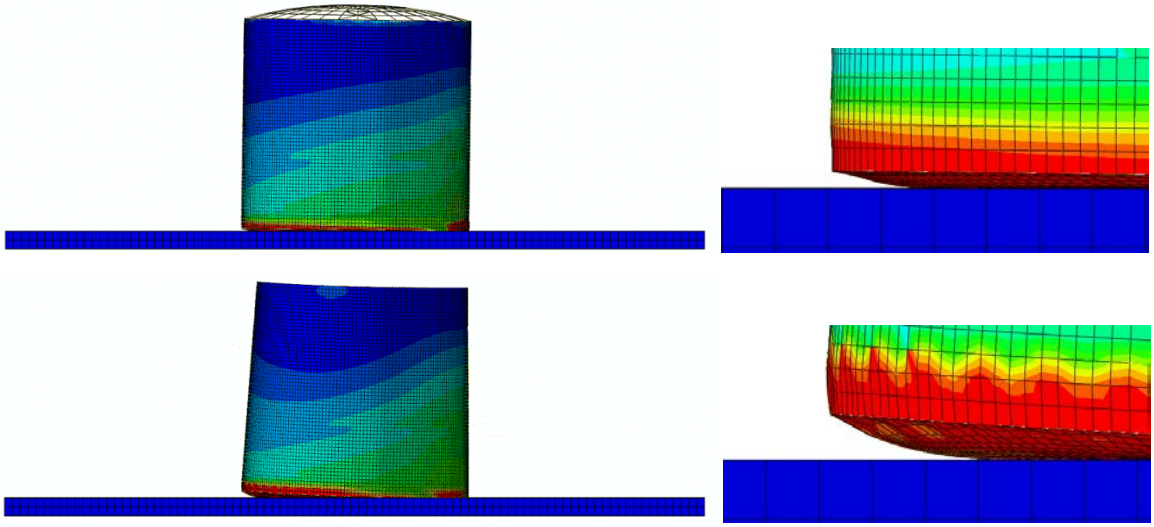

Figure 31: Finite element modeling of the tank with aspect ratio equal to 1.538; (a) with roof, (b) without roof.

4. CONCLUSIONS

The structural behavior of unanchored tanks exhibiting uplifting under severe dynamic (seismic) horizontal excitation has been examined, focusing on the response of the connection between the base

plate and the tank shell. A systematic methodology has been proposed for analyzing unanchored tank response under lateral seismic excitation, towards assessing base plate connection strength against failure due to excessive local strain and fatigue.

More specifically, a nonlinear simplified model is developed and employed for the analysis of the tank under seismic excitation, where the tank is simulated as an equivalent spring-mass mechanical system. Furthermore, to determine the relationship between the overturning moment and the uplifting (rocking) angle, as well as the relationship between the uplifting size and length, a lateral-load static analysis has been performed, using a nonlinear elastic-plastic finite element model.

The proposed model, upon calculation of the global tank seismic response, is capable of estimating the maximum bending strain at the plate-shell connection, through an efficient fatigue analysis of the connection, which considers the strain-range fatigue spectrum of the seismic action, an appropriate $\Delta\varepsilon - N$ low-cycle fatigue curve, and a fatigue damage accumulation factor based on Miner's rule.

The above methodology has been applied on two typical liquid storage tanks and the results indicate a significant effect of uplifting on unanchored tank response, when compared with the case of anchored tanks. Finally, a numerical parametric study of eight unanchored tanks with different values of aspect ratios has been conducted, demonstrating that the stiffness on tank deformation provided by the presence of a fixed roof may have a significant influence on the uplifting size.

The proposed methodology can be used as an efficient tool for conducting a performance-based design procedure, towards assessing tank strength and minimizing seismic risk in industrial facilities.

ACKNOWLEDGMENTS

This research has been co-financed by the European Union (European Social Fund – ESF) and Greek national funds through the Operational Program "Education and Lifelong Learning" of the

National Strategic Reference Framework (NSRF), Research Funding Program: THALES, Investing in knowledge society through the European Social Fund.

The contribution of European Commission through the Research Fund for Coal and Steel (RFCS), Contract No. RFSR-CT-2014-00025, *Component Fragility Evaluation and Seismic Safety Assessment of "Special Risk" Petrochemical Plants Under Design-Basis and Beyond-Design-Basis Accidents*, project acronym INDUSE-2-SAFETY, is gratefully acknowledged.

REFERENCES

[1] Peek, R. (1988). "Analysis of unanchored liquid storage tanks under lateral loads", *Earthquake Engineering and Structural Dynamics*, Vol 16, No. 7, pp. 1087-1100

[2] Natsiavas, S., Babcock, C.D. (1988). "Behavior of unanchored fluid-filled tanks subjected to ground excitation", *Journal of Applied Mechanics*, ASME, Vol. 55, No. 3, pp. 654-659.

[3] Manos, G. C. (1986). "Earthquake tank-wall stability of unanchored tanks", *Journal of Structural Engineering*, ASCE, Vol. 112, pp. 1863-1880.

[4] Wozniak, R. S. and Mitchell, W. W., (1978). "Basis of seismic design provisions for welded steel oil storage tanks", *Session on Advances in Storage Tank Design*, API 43rd mid-year meeting, Toronto, Canada.

[5] Leon, G. S., and Kausel, E. A. M., (1986). "Seismic analysis of fluid storage tanks," *Journal of Structural Engineering*, ASCE,Vol. 112(1), pp. 1-18.

[6] Myers, P. E. (1997). *Aboveground Storage Tanks*, McGraw-Hill, ISBN 0-07-044272-X.

[7] Cambra, F. J, (1982). *Earthquake response considerations of broad liquid storage tanks*, Rep. UCB/EERC-82/25, Earthquake Engineering Research Center, Richmond, California.

[8] Auli, W., Fischer, F. D., and Rammerstorfer, F. G., (1985). "Uplifting of earthquake-loaded liquid-filled tanks," *Proceedings, 1985 ASME Pressure Vessels and Piping (PVP) Conference*, 98-7, 71-85.

[9] Ishida, K., and Kobayashi, N., (1988). "An effective method of analyzing rocking motion for unanchored cylindrical tanks including uplift," *Journal of Pressure Vessel Technology*, Vol. 110, pp. 76-87.

[10] Malhotra, P. K., and Veletsos, A. S., (1994). "Beam Model for Base-uplifting Analysis of Cylindrical Tanks," *Journal of Structural Engineering*, Vol. 120, No. 12, pp. 3471-3488.

[11] Ahari, M. N., Eshghi, S., and Ashtiany, M. G., (2009). "The tapered beam model for bottom plate uplift analysis of unanchored cylindrical steel storage tanks," *Engineering Structures*, Vol. 31, pp. 623-632.

[12] Peek, R., and Jennings, P. C., (1988), "Simplified analysis of unanchored tanks," *Journal of Earthquake Engineering and Structural Dynamics*, Vol. 16(7), pp. 1073-1085.

[13] Peek, R., (1988). "Analysis of unanchored liquid storage tanks under lateral loads," *Journal of Earthquake Engineering and Structural Dynamics*, Vol. 16(7), pp. 1087-1100.

[14] Haroun, M. A., Badawi, H. S., and Nanda, C. B., (1987). "Nonlinear uplift analysis of crescent-shaped plate," *Proceedings, 1987 Pressure Vessels and Piping (PVP) Conference*, San Diego, California, pp. 317-324.

[15] Haroun, M. A., and Badawi, H. S., (1988). "Seismic behavior of unanchored ground-based cylindrical tanks," *Proceedings, 9th World Conference on Earthquake Engineering*, Tokyo- Kyoto, Japan, Vol. 6, pp. 643-648.

[16] Malhotra, P. K., and Veletsos, A. S., (1994). "Uplifting Analysis of base plates in cylindrical tanks," *Journal of Structural Engineering*, Vol. 120, No. 12, pp. 3489-3505.

[17] Clough, D. P. (1977), "Experimental Evaluation of Seismic Design Methods for Broad Cylindrical Tanks,"U.C. Berkeley, Report No. UCB/EERC-77/10

[18] Niwa, A. (1978), "Seismic Behavior of Tall Liquid Storage Tanks," U.C. Berkeley, Report No. UCB/EERC-78/04

[19] Clough, R. W., and Niwa, A. (1979), "Static Tilt Tests of a Tall Cylindrical Liquid Storage Tank," U.C. Berkeley, Report No. UCB/EERC-79/06

[20] Lau, D. T., and Clough, R. W., (1989). "Static tilt behavior of unanchored cylindrical tanks," Rep. UCB/EERC-89/ll, Earthquake Engineering Research Center. University of California, Berkeley, Calif.

[21] Shih, C. F., (1981). "Failure of Liquid Storage Tanks Due to Earthquake Excitation," PhD thesis, Report No. EERL 81-04, Caltech, Pasadena, CA.

[22] Natsiavas, S. (1988). "An Analytical Model for Unanchored Fluid-Filled Tanks under Base Excitation," *Journal of Applied Mechanics*, ASME, Vol. 55, pp. 648-653.

[23] Natsiavas, S. (1990). "Simplified Models for the Dynamic Response of Tall Unanchored Liquid Containers," *Journal of Pressure Vessel Technology*, ASME, Vol. 112, pp. 124-131.

[24] Natsiavas, S. and Babcock, C. D. (1987), "Buckling at the Top of a Fluid-Filled Tank during Base Excitation", *Journal of Pressure Vessel Technology*, ASME, Vol. 109, No. 4, pp. 374-380.

[25] Malhotra, P.K., and Veletsos, A. S., (1994). "Uplifting Response of Unanchored Liquid-Storage Tanks," *Journal of Structural Engineering*, ASCE, Vol. 120, No. 12, pp. 3525-3547.

[26] European Committee for Standardization (2006), *Silos, tanks and pipelines*, Eurocode 8, part 4, CEN/TC 250, EN 1998-4, Brussels.

[27] Prinz, G. S., and Nussbaumer, A., (2012). "Fatigue analysis of liquid-storage tank shell-to-base connections under multi-axial loading," *Engineering Structures*, Vol. 40, pp. 77-82.

[28] Vathi, M., and Karamanos, S. A., (2017). "Performance Criteria for Liquid Storage Tanks and Piping Systems Subjected to Seismic Loading," *Journal of Pressure Vessel Technology*, ASME manuscript PVT-16-1045, DOI: 10.1115/1.4036916.

[29] Bakalis, K., Fragiadakis, M., and Vamvatsikos, D., (2017). "Surrogate modeling for the seismic performance assessment of liquid storage tanks", *Journal of Structural Engineering*, ASCE, Vol. 143(4): 4016199, DOI: 10.1061/(ASCE) ST.1943-541X.0001667.

[30] Cornell, C. A., and Krawinkler, H., (2000). "Progress and Challenges in Seismic Performance Assessment," PEER Center News, 3(2), p. 1-4.

[31] Yang, T. Y., Moehle, J., Stojadinovic, B., and Der Kiureghian, A., (2009). "Seismic Performance Evaluation of Facilities: Methodology and Implementation," *Journal of Structural Engineering*, ASCE, 135(10), p. 1146-1154, DOI: 10.1061/(ASCE)0733-9445(2009)135:10(1146).

[32] Ju, S., and Jung, W. Y. (2013). "Evaluation of Performance Requirements for Seismic Design of Piping System", *International Journal of Civil, Environmental, Structural, Construction and Architectural Engineering*, Vol. 7, No. 2.

[33] Bursi, O. S., Reza, M.S., Abbiati, G., Paolacci, F. (2015). "Performance-based earthquake evaluation of a full-scale petrochemical piping system", *Journal of Loss Prevention in the Process Industries*, Vol. 33, pp. 10-22.

[34] Fragiadakis M., Vamvatsikos D., Lagaros N., Karlaftis M., and Papadrakakis M. (2015). "Seismic Assessment of Structures and Lifelines.", *Journal of Sound and Vibration*, Vol. 334, pp. 29-56.

[35] Vamvatsikos D., Kazantzi A., and Aschheim M.A. (2016). "Performance-based seismic design: Avant-garde and code-compatible approaches.", *ASCE-ASME Journal of Risk and Uncertainty in Engineering Systems, Part A: Civil Engineering*, Vol. 2, No. 2, Paper No. C4015008.

[36] Bursi, O. S., Paolacci, F., Reza, M. S., Alessandri, S., Todini, N. (2016). "Seismic Assessment of Petrochemical Piping Systems Using a Performance-Based Approach", *Journal of Pressure Vessel Technology*, ASME, Vol. 138, No. 3, Article Number: 031801.

[37] Koike, T., Imai, T., and Ogikubo, T. (2008). "Performance-Based Design of Steel Tanks Under Seismic Risks.", *14^{TH} World Conference on Earthquake Engineering*, Beijing, China.

[38] O' Rourke, M. J., Eeri, M., and So, P. (2000). "Seismic Fragility Curves for On-grade Steel Tanks," *Earthquake Spectra*, Vol. 16, New York, USA.

[39] Fabbrocino, G., Iervolino, I., Orlando, F., Salzano, E. (2005). "Quantitative Risk Analysis of Oil Storage Facilities in Seismic Areas," *Journal of Hazardous Materials*, Vol. 123, pp. 61-69.

[40] Salzano, E., Iervolino, I., Fabbrocino, G. (2003). "Seismic Risk of Atmospheric Storage Tanks in the Framework of Quantitative Risk Analysis," *Journal of Loss Prevention in the Process Industry*, Vol. 16, pp. 403-409.

[41] Cortes, G., and Prinz, G.S., (2017). "Seismic fragility analysis of large unanchored steel tanks considering local instability and fatigue damage," *Bulletin of Earthquake Engineering,* Vol. 15(3), pp. 1279-1295, DOI: 10.1007/s10518-016-9984-6.

[42] Ibrahim, R., (2005). *Liquid Sloshing Dynamics: Theory and Applications*, Cambridge University Press, Cambridge, UK.

[43] Veletsos, A. S., and Yang, J. Y. (1977). "Earthquake Response of Liquid Storage Tanks", 2nd Engineering Mechanics Conference, ASCE, Raleigh, NC, pp. 1-24.

[44] Pappa P., Vasilikis, P., Vazouras, P., and Karamanos, S. A. (2011). "On the seismic behaviour and design of liquid storage tanks", III ECCOMAS Thematic Conference on Computational Methods in Structural Dynamics and Earthquake Engineering (COMPDYN), Corfu, Greece, 26–28 May 2011.

[45] Vathi, M., and Karamanos, S. A. (2014). "Modeling of Uplifting Mechanism in Unanchored Liquid Storage Tanks Subjected to Seismic Loading", 2nd European Conference on Earthquake Engineering and Seismology (2ECEES), 24-29 August 2014, Istanbul, Turkey.

[46] Vathi, M., and Karamanos, S. A. (2014). "Liquid Storage Tanks: Seismic Analysis," *Encyclopaedia of Earthquake Engineering*, Article: 368990, Chapter: 144, Springer.

[47] Vathi, M., and Karamanos, S. A. (2015). "Simplified Model for the Seismic Response of Unanchored Liquid Storage Tanks," *Proceedings of the ASME 2015 Pressure Vessels & Piping Division Conference,* PVP2015, July 19-23, 2013, Boston, Massachusetts, USA.

[48] Bathe, K-J, (1996). *Finite Element Procedures*, Prentice Hall Inc., New Jersey.

[49] van der Vegte, G. J., de Back, J., Wardenier, J., (1989). *Low Cycle Fatigue of Welded Structures*, Stevin Report, 25.6.89.09/A1, Delft University of Technology, The Netherlands.

[50] Karamanos, S. A., Romeijn, A., and Wardenier, J., (2000). "Stress concentrations in tubular gap K-joints: mechanics and fatigue design," *Engineering Structures*, Vol. 22, pp. 4-14.

[51] American Petroleum Institute (2007). *Seismic Design of Storage Tanks*, Welded Steel Tanks for Oil Storage, Appendix E, API 650, 11th Edition, Washington, D.C.

[52] Scharf, K., (1990). *Beiträge zur Erfassung des Verhaltens von erdbebenerregten, oberirdischen Tankbauwerken*, Fortschritt-Berichte VDI, Reihe 4. Bauingenieurwesen, Nr. 97, VDI Verlag, Düsseldorf [in German].

[53] Kaufmann, E. J., Metrovich, B., and Pense, A. W., (2001). *Characterization of Cyclic Inelastic Strain Behavior on Properties of A572 Gr. 50 and A913 Gr. 50 Rolled Sections*, Final Report to American Institute of Steel Construction, ATLSS Report No. 01-13.

[54] British Standards Institution (1993). *Fatigue Design and Assessment of Steel Structures*, British Standard BS 7608, UK.